Arctic total water vapor
Improving retrieval methods

Raul Scarlat

A thesis submitted to the Institute of Environmental Physics for the award of the degree of Master of Science in Environmental Physics

Institute of Environmental Physics

University of Bremen

August 3, 2012

Abstract

Water vapor is a component of the atmosphere which plays a critical role in the global climate mechanism. Monitoring the amount and tracking the variability of water vapor in the atmosphere on a global scale is a necessity in order to achieve better short term weather prediction and to understand long term climate change. The polar regions pose a specific set of problems to atmospheric water vapor retrieval. Algorithms have been developed that can measure atmospheric water vapor content in these areas using space-borne microwave radiometers. In this thesis we aim to improve on the methods that are already in place. By performing comparisons with complementary retrieval sources for the Arctic region, a multi-instrument approach to improving retrieval coverage is presented. Also, starting from a tested method for water vapor retrieval in the central Arctic, an extension is proposed that would enable it to also cover open ocean areas.

Contents

List of Figures

Chapter 1

Introduction

1.1 What is water vapor

The planet Earth is able to support life because of a key component within its climate system that sets it apart from other known places in the Universe, a working water cycle. This hydrological cycle characterizes the continual movement of water in all three phases between the planetary atmosphere, oceans and landmasses. Although the large liquid water oceans and the solid ice caps in the polar regions are the most visible components, the gaseous water vapor is an important component in this system. Water vapor provides the link between the large liquid water reservoir that is the planetary ocean and the liquid water clouds that bring precipitation over the continents. The basic workings of the hydrological cycle are known, but some interactions that concern its water vapor component are still not understood primarily because of insufficient observations of atmospheric water vapor.

Another mechanism that allows life to thrive on this planet is the greenhouse effect of Infra-Red (IR) absorbing gases in the atmosphere. This mechanism keeps the surface temperature high enough to ensure a life-friendly climate. There are a number of greenhouse gases in the atmosphere, some natural and other of anthropogenic origin, but the most important of these is water vapor. Because of the intrinsic characteristics of the water molecule, water vapor absorbs strongly in the long wave spectrum. The atmospheric saturation vapor pressure is proportional with the air temperature so that warmer air has a higher saturation vapor pressure and can therefore hold more water vapor before it condensates to liquid. Due to its behavior as a greenhouse gas and because of the link between air temperature and water vapor load, it can play an important role in a positive feedback process within the atmosphere. Once a warming process is started, the higher air temperature allows more water to evaporate, and the resulting water vapor drives the warming process in the atmosphere further because of the greenhouse effect. Besides this simplistic explanation, the behavior of water vapor in the atmosphere is far more complex as it interacts with clouds, with the incoming short-wave and the outgoing long wave radiation, all while being part of the general atmospheric circulation. Some of the aspects of these interactions are still not understood also because of a lack of observation data about atmospheric water vapor.

1.2 Water vapor terminology

Water in its gaseous form is simply called water vapor. The climatological parameter water vapor can be quantified in a number of different ways, depending on the context of application. For meteorologists it can be expressed as the actual concentration in a fixed volume of air, or it can relate to the maximum amount required to saturate the air. Saturation occurs when adding more water vapor to the volume of air would cause it to condensate to liquid. When saturation is achieved, the rate at which water molecules are added through evaporation is equal to the rate at which they leave the air parcel by condensation.

By relating the quantity of water vapor to the overall quantity of air in the sample we define the samples specific humidity, and by relating the amount of water vapor only to the amount of dry air in the sample we define the mixing ratio. Both of these quantities are dimensionless numbers, but because of the small concentration of atmospheric water vapor (in places even below 1%), these quantities can be expressed in units of grams of water vapor per kilograms of air (moist or dry).

Vapor pressure defines the partial pressure for which only the water vapor in moist air is responsible. Saturation vapor pressure is the pressure needed to achieve air saturation and is directly linked to the air temperature. It follows a rapid increase with temperature, doubling between 21 ^{o}C and 32 ^{o}C. This phenomenon characterizes the connection between the atmospheric water vapor load and air temperature. Relative humidity is expressed as a percentage and represents the ratio of the vapor pressure to the saturation vapor pressure. It is important to note that two parcels of air of different temperature can have the same relative humidity but different water vapor content, because of the dependence of the saturation vapor pressure on temperature.

Throughout this thesis, when we are referring to the water vapor content of the atmosphere it will be expressed as total columnar water vapor, or in short total water vapor (TWV). This represents the mass of water vapor in a column of air over a 1 m^2 area, integrated over the entire height of the atmosphere. TWV is equivalent to total precipitable water vapor which is the height to which the water level would rise if all atmospheric water vapor would precipitate down. TWV is measured in kg/m^2 and is numerically equal to the total precipitable water vapor expressed in mm of height.

1.3 Mean distribution of water vapor

When considering the entire mass of the atmosphere, water vapor would only count for 0.25% of the total sea level pressure of atmospheric gases. The total water vapor load of the atmosphere, if evenly distributed around the globe, would amount to about 25 kg/m^2.This is a global average, but because of different atmospheric conditions, the distribution of water vapor is not even, and so in equatorial regions it would amount to 60 kg/m^2 and less than a tenth of that at the poles. When it comes to the temporal variability of atmospheric water vapor concentration, the average precipitation around the globe is about 1 m per year which means that the cycling of water in the air in gas and liquid form is fast, the average residence time for one water molecule in the atmosphere is about 9 days.

Water vapor is not only unevenly distributed horizontally across the planet but also vertically. The concentration of water vapor in the atmosphere is influenced by the air temperature and as it varies with height and across geographical features so does the distribution of water vapor. Almost 50% of the entire mass of water vapor is found below 1.5 km above sea level [25]. Despite the small amount of water vapor in the upper troposphere (above about 5 km) and stratosphere, research has shown that upper tropospheric water vapor plays an important, but not yet fully understood role in the climate [1].

A more detailed look at the global horizontal distribution of atmospheric water vapor is presented in Figure 1.1 Here also, atmospheric water vapor load follows the general surface temperature distribution, with the highest values occurring in equatorial regions and, decreasing with latitude, the lowest values occurring near the poles. Latitude and surface temperature are not the only factors influencing the atmospheric water vapor content, as the major warm desert regions and high mountain ranges are exceptions for the lower latitudes. Atmospheric circulation brings warm, dry air over areas such as the Sahara desert, and because most water vapor is concentrated in the lowest 5 km of an atmospheric column, over high geographical features the column of air that can effectively hold water vapor is much shorter thus leading to a lower water vapor load then in low level areas at the same latitude. Consequently, above the equatorial oceans high air temperature, coupled with the huge evaporation sources and convective atmospheric movement determine the highest water vapor load in Earth's atmosphere.

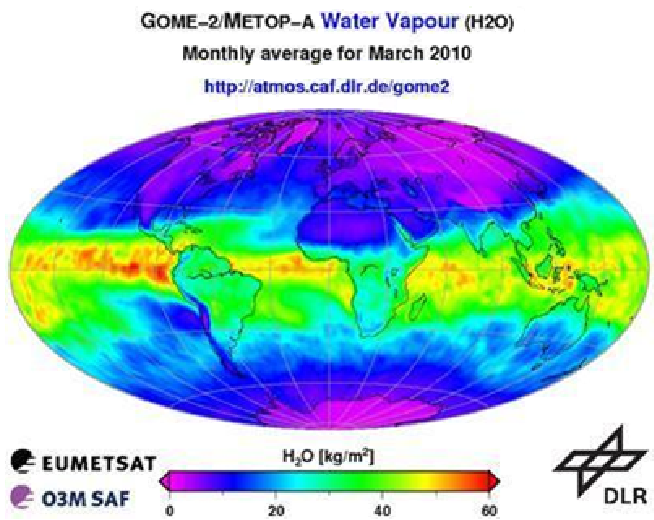

Figure 1.1: Global mean horizontal distribution of atmospheric water vapor (NASA image)

1.4 Temporal variability of water vapor

As stated before, variability is one of the most important characteristics of the atmospheric water vapor. Following seasonal patterns and the routes of general atmospheric circulation, the water vapor load varies on time scales raging from minutes to decades. Because of the influence of landmasses and the corresponding temperature changes, seasonal variations are more strongly felt in the northern hemisphere. The higher fraction of ocean in the southern hemisphere acts as a buffer for rapid temperature variations, thus leading to a more temporally stable atmospheric water vapor distribution. On the timescale of a few years, the El-Nino Southern Oscillation phenomenon induces changes in the tropical Pacific sea surface temperature, and the water vapor distribution changes accordingly.

1.5 Water vapor trends

The study of long time water vapor records has provided an insight into the trends of water vapor variability within the troposphere. Some recent studies show an increasing trend for atmospheric water vapor. A global ocean trend for the time period 1988 to 2003 is estimated to an increase of $1.3\pm 0.3\%$ per decade [2]. Generally, positive trends were found in regions where rising temperature trends were also recorded during the same period, an important remark in the current global warming scenario.

A decades long record of monthly measurements from weather balloons launched in the area of Boulder, Colorado show an increase in the local stratospheric water vapor content of approximately 1% per year between 1980 and 2004 [3]. Quantitatively the stratospheric water vapor load increased by $27\pm6\%$ during 1980-2010 while showing relatively large short-term variations throughout the period (shown in Figure 1.2). The increasing trend is more stable at higher altitudes indicating the action of mechanisms that strengthen with increasing altitude such as methane oxidation. Although the amount of oxidized methane has also increased in the same time period, this mechanism alone can only account for $25 \pm 5\%$ of the water vapor increase for the entire 30 years period [4].

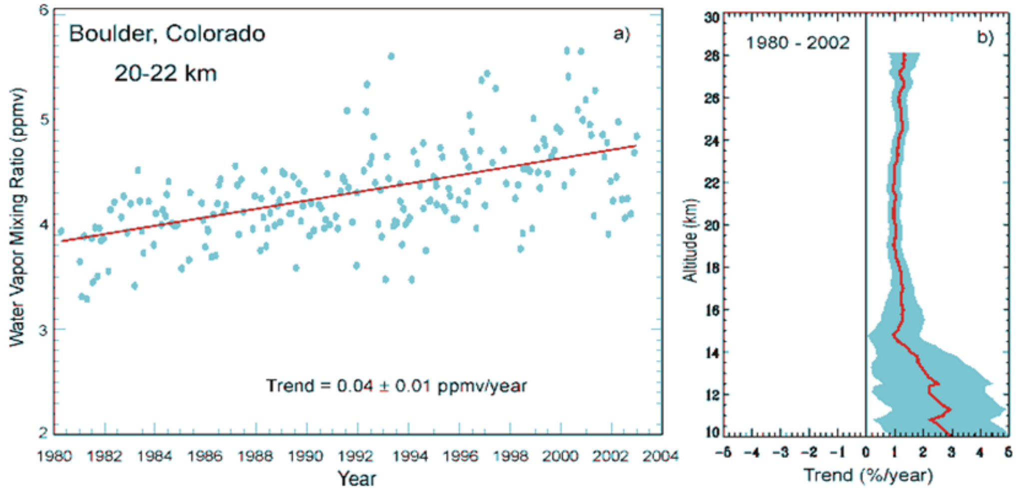

Figure 1.2: Water vapor trends as measured from balloon frost-point hygrometers. a) Increasing trend for the 20-22 km atmospheric layer, between 1980 and 2004. b) Trend for the stratospheric vertical profile between 10 and 30 km altitude [23].

1.6 The role of water vapor in the climate system

As mentioned before, water vapor provides the connection between surface and the atmosphere within the hydrological cycle. As is shown in Figure 1.3, most of the atmospheric water vapor originates on the planet surface, where it is released from surface evaporation and from biological processes. Following the circulatory patterns of the atmosphere, depending on the local conditions of air pressure and temperature, vapor will condense to water, forming clouds. If precipitation is formed, then the water returns to the surface to complete the cycle.

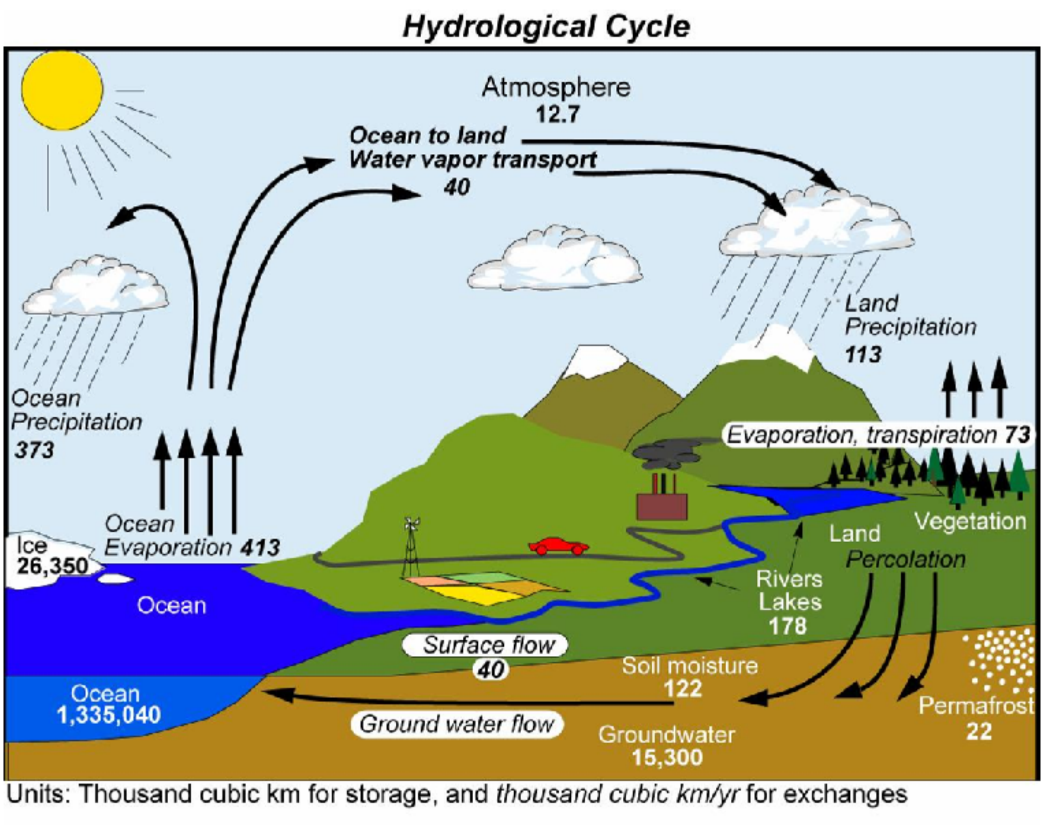

Figure 1.3: The global water cycle [2].

As a component of the climate system, the water cycle is closely tied to local temperature. The ocean surface temperature varies more slowly than land surface temperature, and other factors such as soil moisture can contribute to a high variability in the water transport system.

Water evaporation happens all across the planet surface but at very different rates. Over land the predominant phenomenon is precipitation followed by the outflow of water through rivers into the oceans. To balance this system, most evaporation happens over the oceans from where water vapor is continuously carried inland where it condenses and precipitates down again.

Besides transporting water between oceans and land, the hydrological cycle fulfills an important task within the climate system. During its journey from source to sink, water vapor also transports latent heat within the atmosphere. This is the energy the water molecules needed to absorb in order to leave the more stable state of liquid and be released as gas. The energy thus acquired through evaporation is released again when water vapor condenses, usually at great distance from the original location where evaporation took place. This mechanism provides energy for weather systems all across the globe.

1.7 The role of clouds

One of the least understood components of the hydrological cycle is the action of clouds. They act to reflect solar radiation because of their high albedo, but being made up of water they also strongly absorb the IR radiation of the planet surface. Therefore clouds can have both a cooling and a warming effect in the atmosphere. Because cloud cover is subject to rapid change, they will contribute to the effects of unequal heating of the Earths surface and so influence the rate of surface evaporation and convective heat transport. These local variations in evaporation rates influence in turn cloud formation. Another link in this complex system is the precipitation connected to clouds which will also influence soil moisture over land and the surface evaporation rate. Soil moisture and the amount of solar radiation that reaches the surface are the most important factor for plant life development, and the presence of plants can sustain further development of the local biotope. The biological component of the water cycle is also responsible for water vapor release in the atmosphere, i.e. from perspiration and evaporation. Because of the complex interconnections between all of these components, it is hard to predict if the net effect of clouds will be to amplify or buffer climate change in the future.

Cloud updraft is believed to be responsible for transporting water vapor into the upper troposphere, but the whole mechanism is not completely understood. Cloud microphysics and large scale cloud dynamics are thought to lead to a drying of the higher troposphere. Models so far indicate that large storm systems and cloud processes are the primary force behind water vapor transport into the higher troposphere but the exact working of this complex system is not certain and more observation data are required for improving and testing models [4],[5].

1.8 Water vapor retrieval

To enable monitoring of water vapor in the atmosphere, a number of retrieval methods have been developed, each with their weak points and advantages. In Figure 1.4, different types of monitoring systems are shown that are currently in use for atmospheric water vapor content measurements.

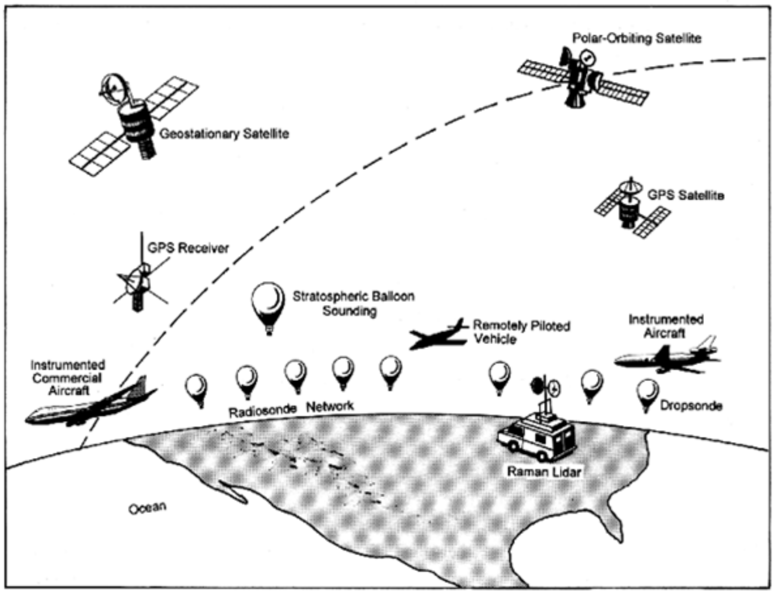

Figure 1.4: Ground-, air- and space-borne methods for water vapor retrieval [2]

The most reliable retrieval source for water vapor information will remain the hygrometer observations taken routinely at meteorological stations. These provide long records with high temporal resolution and good quality observations but the fact that the meteorological station network is unevenly distributed around the globe as well as the fact that the data is relevant for the bottom part of the troposphere reduce the applicability of this method.

To improve on the vertical resolution of water vapor measurements, since the 1930s, sounding equipment was launched in balloons. This method provides a relatively cheap source of data that has provided long records for locations around meteorological stations. This means that coverage beyond the station locations is not achievable. Data quality depends on the instruments used and the retrieval does not include the higher troposphere.

For research purposes, more sensitive instruments can be deployed such as surface radiometers. Microwave and IR radiometers can both deliver high quality data but, while microwave instruments suffer from poor vertical resolution, IR retrieval is hampered by cloud cover. The number of such instruments is restricted by the high cost of a single unit.

Aircraft-mounted instruments can record water vapor data with better coverage than surface methods, but aerial campaigns are expensive and the duration of one flight during witch measurements can be taken is on the order of hours. Plans to mount instruments on commercial aircraft that would ensure constant measurements between airport locations have not been implemented on a scale large enough to achieve operational status [19].

For daily monitoring on a global scale, satellite retrieval provides the best option. IR sensors like TOVS can obtain integrated atmospheric water vapor load and low resolution vertical profiles because of the wide satellite footprint [18]. The temporal resolution is affected by data corruption from cloud cover. Microwave imagers such as AMSR-E (Advanced Microwave Scanning Radiometer for EOS) and SSM/I (Special Sensor Microwave/Imager) are only little affected by clouds but the retrieval is normally limited to the ice-free oceans because the surface emissivity component from ice, snow and the various land surfaces cannot be completely compensated for. The microwave imagers do not allow to retrieve information about the vertical distribution of water vapor; they only give column integrated values. Vertically resolved water vapor information can be obtained with sounders, like AMSU-B (Adnvanced Microwave Sounding Unit)or MHS (Microwave Humidity Sounder). In the case of sounders however, the vertical resolution is low. For retrieving information about the highest layers of the atmosphere with good vertical resolution, sensors using solar occultation methods like SAGE (Stratospheric Aerosol and Gas Experiment) II are used. A drawback of retrieving from this position (through the limb of the Earth's atmosphere) is that cloud cover can severely affect retrieval, especially in lower latitudes [20].

By special processing of the signal delay from different GPS satellites, information about the water vapor content of the atmosphere can be retrieved. A good vertical resolution can be achieved, but the presence of receivers on the ground is necessary and limits coverage.

Covering the observational gap would lead to a better understanding of the exact role of water vapor within the climate system. Until the last decade most climatological studies on water vapor have been based on radiosonde retrieval which offer good vertical resolution for the lower troposphere but only offer coverage for populated regions where the density of meteorological stations is high enough, but these retrievals shed no light on remote regions like oceans and polar caps.

In recent years, satellite observations from microwave and IR radiometers have encountered more success in achieving wide coverage while providing reasonable resolution for water vapor retrieval. Although useful, these methods cannot achieve permanent global monitoring because they are restricted by weather conditions and surface types. Where there are no real life observations available data assimilation systems, like the ECMWF (European Centre for Medium-Range Weather Forecast) model products, can complete the image by combining measurement data where possible with output from atmospheric models.

Models of the hydrological cycle can provide more insight into the workings of the global climate system as well as more practical improvements in short term weather forecasting (like the Global Energy and Water Cycle Experiment GEWEX project of the World Climate Research Programme) [21]. Improved water vapor data would help modelling efforts by providing accurate training information for simulating water vapor interactions in the atmosphere as well as validation possibilities for simulated water vapor distributions.

On a planetary scale the use of complementary retrieval methods for particular regions and the subsequent combination of sources can yield more useful information than generalizing one single method for global applicability.

1.9 Challenges for retrieval in the Arctic

The Arctic region is one of the most extreme environments on the planet. Temperatures range over a very wide range between about -40 and 0 ^{o}C in January and roughly -10 to 10 ^{o}C in July. Precipitations are usually in the form of snow and average 500 mm around the year, which represents half the global average of 1000 mm, but varies locally and depending on season. Some parts of the Arctic (Arctic Basin) are as dry as the tropical deserts, receiving less than 250 mm of precipitation yearly, while others will have three times as much (South of Greenland) [6]. The climate of the Arctic is therefore subject to large variations on a regional and seasonal basis which translates into very visible cyclic changes in the environment such as the seasonal melt and refreeze of the Arctic sea ice cap. Any small change in the climatic parameters beyond the cyclic norm is translated into dramatic changes in the physical environment. Data shows that the temperature has been increasing in the last 3 decades over the northern reaches of Eurasia and North America [7]. As a consequence, sea ice extent has been constantly shrinking [8], snow cover is getting smaller and the glaciers are retreating [9]. As we are faced currently with the prospect of planetary climate change, the most sensitive regions of the planet will be where the most dramatic transformations will take place as any small change in the local climatic parameters can be amplified by natural feedback (e.g. the ice albedo feedback in the Polar Regions).

Because of its extreme location the Arctic is a problematic region for remote sensing applications. Radiosonde retrieval of total water vapor is not sufficient because of the scarcity of weather stations in this area. Satellite retrieval faces also a number of obstacles. Optical sensors face the constant issue of cloud cover and the seasonal lack of sunlight while microwave measurements are impaired by our incomplete understanding of the way in which sea ice behaves at the retrieval frequencies [12].

Chapter 2

Polar TWV retrieval using space-borne microwave radiometer

2.1 Water vapor retrieval over Antarctica

The Miao et al [12] method was the first step in TWV retrieval in polar areas using space-borne microwave radiometers. It used the SSM/T2 sensor and was designed to work in the Antarctic. The key concept is that this method uses several channels with similar surface emissivity but different water vapor absorption behavior. These are the three channels near the 183.31GHz water absorption line, which together with the channel at the 150GHz window frequency can retrieve TWV values up to about 7 kg/m^2. Above this value two of the band channels become saturated and the signal does not pass through to the ground anymore. This algorithm works well for the Antarctic because the atmosphere is dry enough throughout the year. In the Arctic, the summer months mean higher TWV loads as a combination of moist air advection from lower latitudes, higher air temperatures and the presence of more open ocean area that represents a water vapor source push the TWV load high above the 7 kg/m^2 limit. This is why, in [10] a method is proposed that builds upon the Miao algorithm and provides and extended range for better retrieval in the Arctic. Using the same pairing of channels as the Miao algorithm, the Melsheimer, Heygster method can achieve the same retrieval range in the Arctic, and by also recruiting the 89 GHz channel the range of values can be extended up to 15 kg/m^2 with reasonable accuracy. The original Miao algorithm dealt with the problem of uncompensated surface emission by assuming the same surface emissivity for all channel frequencies. This assumption cannot hold if the 89 GHz channel is also used and then some information about the type of surface has to be included into the retrieval. The Melsheimer, Heygster algorithm can retrieve TWV up to 7 kg/m^2 independent on surface type and up to 15 kg/m^2 only over sea ice. Because the proportion of sea ice and open ocean is constantly varying in the Arctic, the purpose of this paper is to propose a method to further extend this algorithm to enable it to retrieve TWV for the maximum possible range also above open water.

2.2 The original idea

The retrieval equation derivation follows the path described in [9] and is given here for the purpose of better explaining the improvement proposed in Section 3.4. A down looking microwave radiometer will measure upward radiances at the top of the atmosphere. These radiances can be approximated to brightness temperatures of the Earths surface. Using the linear Rayleigh-Jeans approximation we express the radiance measured by the instruments as the brightness temperature:

$$T_b(\theta) = m_p T_s - (T_0 - T_c)(1 - \epsilon)e^{-2\tau sec\theta} \tag{1}$$

Were θ is the viewing angle of the satellite, mp is a correction factor that accounts for the effect of deviation from isothermal atmosphere and difference between surface and air temperature. Ts is the ground surface temperature, Tc the brightness temperature of the cosmic background contribution, T_0 is the ground level atmospheric temperature.ϵ is the problematic surface emissivity, while the is the atmospheric opacity. This is an exact equation so if the exact values for each parameter are plugged into the equation we would get the exact value of the brightness temperature. Even if each component of the temperature signal could be exactly determined, the mp correction factor has to be approximated. For the ideal model of a isothermal atmosphere, the ground is a specular reflector and the ground skin temperature being equal to the ground level atmospheric temperature, mp would be 1. The Melsheimer, Heygster algorithm assumes the ground to be a specular reflector which is a sufficient approximation for remote sensing applications in the microwave domain [16].

The principal idea of the original technique was to take the brightness temperature measurements from three channel frequencies were the ground component would be the same and find the link between these brightness temperatures and the water vapor load of the atmosphere. This would be the retrieval equation for the classical case (Miao algorithm). The extended algorithm will use a different retrieval equation because the three channels with equal emissivities are not available for the higher range TWV values. In this case information about the surface type will be integrated into the retrieval.

2.3 The retrieval equation for the classical case

In this initial scenario, the algorithm uses the band channels around 183.31 GHz from a sensor system like SSM/T2 (Special Sensor Microwave/Temperature & Humidity Profile) or AMSU-B. As long as no channel is saturated [1] all channels see the ground and the emissivity is the same for all three measurements. The water vapor absorption will be different for the three channel frequencies. If i,j,k is the increasing order of channel frequencies (i.e. $\nu_i < \nu_j < \nu_k$) then the mass absorption coefficients will be $k_i < k_j < k_k$. To cover the whole retrieval range, the original algorithm used two combinations of channel triplets: i) 183.31±7, 183.31±3, and 183.31±1 GHz (AMSU-B channels 20, 19, 18); or ii) 150, 183.31±7, and 183.31±3 GHz (AMSU-B channels 17, 20, 19). For the first channel combination the assumption of equal emissivity is well matched to reality because the three frequencies are so close to each other. For the second pairing, the same assumption is still used although the in frequencies is greater and some inaccuracy is introduced in the retrieval. In the original paper [12], it is argued that using this assumption for the second channel triplet represents a small error source when compared to other ones. Quantitatively it is shown in Wang et al [14], Selbach [11] and Selbach et al [15] show that using the same emissivity assumption while including the 150 GHz channel will cause a positive bias of up to 0.5 kg/m^2 depending on the type of ice at the surface. Further, we give a short outline of the original algorithm as described in [10]. This is important in order to make the connection with the modified retrieval equation described in [**?**]. Starting from the expression of brightness temperature given in (1), if we want to simplify it we can take the difference

[1]the channel signal comes from the upper layers of the atmosphere and does not include any information about the surface

of two brightness temperatures measured at two different channels i, j and we get:

$$\Delta T_{ij} \equiv T_{b,i} - T_{b,j}$$

$$\Delta T_{ij} = (T_0 - T_c)(1-\epsilon)(e^{-2\tau_j sec\theta} - e^{-2\tau_i sec\theta}) + b_{ij} \tag{2}$$

We can see that in (2) the free T_s term has disappeared. To account for the differences in the m_p term, the bias term b_{ij} was introduced.

$$b_{ij} = T_s(m_{p,i} - m_{p,j}) \tag{3}$$

As shown in [10] - Appendix II, good approximation for this term is:

$$b_{ij} \approx \int_0^\infty [e^{-\tau_j(z,\infty)sec\theta} - e^{-\tau_i(z,\infty)sec\theta}]\frac{dT(z)}{dz}dz \tag{4}$$

Here, T(z) stands for the temperature profile of the atmosphere with height z. To obtain a relationship between the measured brightness temperature and the absorption due to water vapor we require the third brightness temperature measured on channel k. With this, a pair of brightness temperature differences is available from which the ratio will be:

$$\frac{\Delta T_{ij} - b_{ij}}{\Delta T_{jk} - b_{jk}} = \frac{e^{-2\tau_i sec\theta} - e^{-2\tau_j sec\theta}}{e^{-2\tau_j sec\theta} - e^{-2\tau_k sec\theta}} \tag{5}$$

For ease of notation we can follow the naming convention in [10] and use for the left hand side of (5) the ratio of compensated brightness temperatures, η_c (containing the correction terms b_{ij}, b_{jk}). η_c is fully independent of any surface contribution, and only influenced by the atmospheric opacity terms $({}_{i}, {}_{j}, {}_{k})$ at the three channel frequencies. Each opacity term is a function of the amount of absorption by water vapor and oxygen and can be expressed as:

$$\tau_i = k_{vapor,i}W + \tau_{oxygen,i} \tag{6}$$

Where $k_{vapor,i}$ is the mass absorption coefficient for water vapor for channel i, ${}_{oxygen,i}$ represents the oxygen contribution to the atmospheric attenuation at channel i, and W is the water vapor load. For the channels around the 183.31 GHz frequency, the contribution of water vapor to the absorption is much stronger than for oxygen so that the $_{oxygen,i}$term can be neglected.

The aim is to have a direct connection between the ratio of brightness temperature and the water vapor content W. Using the approximation introduced in [13], the difference of exponentials can be transformed into a product of a linear and an exponential function so that eventually we get:

$$\eta_c = exp[B_0 + B_1 W sec\theta + B_2 (W sec\theta)^2] \tag{7}$$

Where B_0,B_1, and B_2 depend on the mass absorption coefficients k for the three channels and are called bias parameters. When compared to the first two terms under the exponent, the quadratic term can be neglected so that when we take the logarithm of (7) we have:

$$log\eta_c = B_0 + B_1 W sec\theta \tag{8}$$

The final retrieval equation for water vapor content W is then

$$W sec\theta = C_0 + C_1 log\eta_c \tag{9}$$

The constant parameters C_0 and C_1 are related to B_0 and B_1 and characterize the atmospheric attenuation at the used channel frequencies, and they are determined from simulated brightness temperatures. As the atmospheric conditions vary throughout the globe, these simulations are run using ARTS (Atmospheric Radiative Transfer Simulator)[17] for atmospheric profiles of the Arctic atmosphere retrieved from radiosonde measurements.

2.4 Finding the calibration parameters

By replacing the form of θ_c from (7) in the ratio of brightness temperature differences (5) we obtain the linear relationship between ΔT_{ij} and $\Delta T_P jk$

$$\Delta T_{ij}(\epsilon) = b_{ij} + \eta_c(W)(\Delta T_{jk}(\epsilon) - b_{jk}) \tag{10}$$

The brightness temperature differences depend on the surface emissivity while η_c only depends on W. In a ΔT_{ij} vs ΔT_{jk} scatter plot, with constant W and for varying ϵ, equation (10) describes a straight line of slope η_c(W) that runs through the point (b_{ij}, b_{jk}). Because the two bias parameters vary only weakly with W and η, all lines obtained for different W values will cross or pass very near to one single point $F(F_{jk}, F_{ij})$, called focal point in [12]. To find the focal point coordinates, brightness temperature simulations were run for 11 discrete values of . For each simulation, realistic W values are provided from radiosonde profiles of Arctic atmospheric conditions. For all simulations, the surface temperature is taken to be the ground level atmospheric temperature. After fitting the lines corresponding to each W in the scatter plot, the point of least square distance from all of them will be the focal point. By finding the focal point coordinates we know the correspondence between the simulated brightness temperature differences and the W values and so fit equation (9). From this fit, the constant calibration parameters C_0 and C_1 are retrieved. With this method a total of four parameters, two focal point coordinates and two atmospheric calibration parameters, are derived through the regression fit. The principal problem with the original algorithm of Miao et al. [11], was that the sensitive band channels around the 183.31 GHz frequency will reach saturation with relatively low amounts of atmospheric water vapor. This means that after crossing a certain threshold value for W, the temperature T does not vary with increasing W. The relationship between W and T_b is the functioning principle of the entire algorithm. Therefore, when one channel reaches the W value when it saturates it cannot be used in the retrieval triplet for higher W values. For the first channel triplet (183.31 ±7, 183.31±3, and 183.31±1 GHz), the first channel (AMSU-B channel 18 at 183.31±1 GHz) reaches saturation at 1.5 kg/m^2. To achieve a practical W retrieval range, for values higher than 1.5 kg/m^2 the channel triplet (17, 20, 19 - 150, 183.31 ± 7, and 183.31 ± 3 GHz) is used and can function up to 7 kg/m^2 when channel 19 reaches saturation. For a practical value when the algorithm should switch between the two channel triplets, the saturation point for a given channel k, as defined in [12], is the W threshold value after which $T_{b,j} \leq T_{b,k}$, or simply

$$T_{b,j} - T_{b,k} > 0 \tag{11}$$

To stretch out the retrieval range, the above condition can be relaxed. If originally the saturation cutoff temperature is 0 $T_{bj} - T_{b,k} \geq 0$, this can be modified into using the saturation cutoff to $F_{20,19}$ ($T_{bj} - T_{b,k} \geq F_{20,19}$), with $F_{20,19}$ being a few Kelvins. This modification translates into an increase in the retrieval range of values by about 1 kg/m^2. The disadvantage derived from this is that the retrieval error increases as the channel approaches its saturation limit. If the difference $\Delta T)jk - F_{jk}$ is smaller than 10 K the corresponding error for the second channel triplet (17, 20, 19) is below 0.4 kg/m^2 for the retrieval range 1.5 7 kg/m^2. For the first channel pairing (20, 19, 18) which has the narrow retrieval range of 0 1.5 kg/m^2 the error is below 0.2 kg/m^2.

2.5 An extended algorithm for TWV retrieval over sea ice

In order to correct the limitation of the original algorithm that could only retrieve TWV values up to 7 kg/m^2 the Melsheimer, Heygster algorithm proposes a modified retrieval method that extends the range up to 14 kg/m^2.

Normally, for TWV values above 7 kg/m^2, saturation occurs at channel 19. A new channel needs to take its place in the triplet which means that a new set of assumptions have to be made about the retrieval. Now, the three channels i, j, k represent AMSU-B channels 16, 17 and 20 (89,150 and 183.31$\pm$7 GHz). Because channel 16 is so far apart from the other two, we can no longer assume that it has the same surface emissivity as the others. Therefore we will have $\epsilon_i \neq \epsilon_j$, for the new channel i, and $\epsilon_j = \epsilon_k$ is the approximation used as before.

If we now consider that we have two channels with different surface emissivities, the brightness temperature difference will now be:

$$\Delta T_{ij} \equiv T_{b,i} - T_{b,j}$$

$$\Delta T_{ij} = (T_0 - T_c)(r_j e^{-2\tau_j sec\theta} - r_i e^{-2\tau_i sec\theta}) + b_{ij} \tag{12}$$

r is here the ground reflectivity $(1-\epsilon)$, and b_{ij} is the same parameter defined in (4) as it does not depend on the surface emissivity ϵ. The corresponding compensated ratio of brightness temperature differences is:

$$\eta_c = \frac{\Delta T_{ij} - b_{ij}}{\Delta T_{jk} - b_{jk}} = \frac{r_i e^{-2\tau_i sec\theta} - e^{-2\tau_j sec\theta}}{r_j e^{-2\tau_j sec\theta} - e^{-2\tau_k sec\theta}} \tag{13}$$

Rearranging terms to resemble the original form in (5) we get:

$$\eta_c = \frac{r_i e^{-2\tau_i sec\theta} - e^{-2\tau_j sec\theta}}{r_j e^{-2\tau_j sec\theta} - e^{-2\tau_k sec\theta}} - \left(-\frac{r_i}{r_j}\right)\left(\frac{e^{-2\tau_j sec\theta}}{e^{-2\tau_j sec\theta} - e^{-2\tau_k sec\theta}}\right) \tag{14}$$

After approximating the difference in exponentials as before the compensated ratio of brightness temperature differences becomes:

$$\eta_c = \frac{r_i}{r_j} exp[B_0 + B - 1W sec\theta + B_2(W sec\theta)^2] - \left(1 - \frac{r_i}{r_j}\right) C(\tau_j, \tau_k) \tag{15}$$

Where

$$C(\tau_j, \tau_k) = \frac{e^{-2\tau_j sec\theta}}{e^{-2\tau_j sec\theta} - e^{-2\tau_k sec\theta}}$$

Is a constant function that depeends only on the atmospheric absorption factors. In order to obtain a simple linear relationship between the compensated brightness temperature difference and water vapor load W we rearrange the above equation into:

$$log\eta\prime_c = B_0 + B_1 W sec\theta + B_2 (W sec\theta)^2 \tag{16}$$

With the modified ratio $\eta\prime_c$ includes the terms depending on the reflectivities and the $C(\tau_j, \tau_k)$ function:

$$log\eta\prime_c = \frac{r_i}{r_j}[\eta_c + C(\tau_j, \tau_k)] - C(\tau_j, \tau_k) \tag{17}$$

The final retrieval equation for W is obtained after eliminating the negligible quadratic term

$$W sec\theta = C_0 + C_1 log\eta\prime \tag{18}$$

The difference between $\eta\prime_c$ and η_c is that the former is not independent of surface emissivity as can be seen from (17). To enable retrieval using equation (18), more information is needed about the behavior of the surface emissivities at the two outermost channel frequencies, 150 and 89 GHz. Using direct information about the surface emissivity for every satellite footprint is not possible so that another alternative is to parametrize the emissivity and obtain a constant reflectivity ratio that would only roughly depend on the surface type (ocean / ice / land). Differentiating between the major surface types in the Arctic is another task that has to be integrated into the algorithm. The Melsheimer, Heygster algorithm extension is adapted only for sea ice surfaces, and excludes all others. The source for the information about surface emissivity came from the Surface Emissivities in Polar Regions-Polar Experiment (SEPOR/POLEX measurement campaign in 2001).

This measurement campaign used an aircraft mounted instrument, the Microwave Airborne Radiometer Scanning System (MARS) which possesses two microwave channels of similar frequencies as the ones required for the algorithm extension. For AMSU-B channel 16 at 89 GHz, there is the MARS channel 88.992 GHz, and for AMSU-B channel 20 at 150 GHz corresponds the MARS channel at 157.075 GHz. This difference of 7 GHz does not pose any significant issues for the retrieval using the 150 GHz channel. According to [10] the difference between measurements at 150 and 157 GHz is between $\pm$ 0.01 from the in situ measurements reported in [16] and [11], while the emissivity variability for the different ice types is greater than this difference. Because of this the impact on the final retrieval is negligible.

2.6 Integrating the emissivity measurements

The measurements in this campaign were carried out above first-year and multiyear sea ice and also above ocean water and land-ice. Because the Melsheimer, Heygster algorithm requires a constant reflectivity ratio, all sea ice is treated as one surface type and open ocean water and land are eliminated from the retrieval with the extended method. To obtain the reflectivity ratio, the regression of ϵ_{89} as a function of ϵ_{150} was calculated

$$\epsilon_{89} = a + b\epsilon_{150} \tag{19}$$

For the ratio of reflectivities to be constant it had to be independent of the variable emissivities. Because of this the regression was constrained so that ϵ_{89} $(\epsilon_{150} = 1) \approx 1$. The physical meaning of this is that the emissivity for the two channels cannot be greater than 1. Using the constraint above means that $a + b \approx 1$ and so the reflectivity ratio only depends on the regression relationship coefficient b

$$\frac{r_j}{r_i} \approx \frac{1}{b} \tag{20}$$

From the data points over sea ice the following regression relationship was found for emissivity at 89 and 150 GHz

$$\epsilon_{89} = 0.1809 + 0.8192 \cdot \epsilon_{150} \tag{21}$$

which determines the reflectivity ratio

$$\frac{r_j}{r_i} = 1.22 \tag{22}$$

It is signalled in [10] that this is just a partial compensation for the contribution of surface emissivity. The SEPOR/POLEX measurements were made in winter season and therefore do not take into account the melt phenomenon that takes place in summer which can significantly alter the emissivity behavior of the surface. Again, because other resources on the subject are sparse, this was the only option to at least include the effects of surface emission into TWV retrieval.

2.7 Calibration parameters for the extended algorithm

Besides the two parameters C_0 and C_1 that account for the atmospheric conditions in the Arctic, the modified ratio of compensated brightness temperatures $\eta\prime_c$ requires the $C(\tau_j, \tau_k)$ term that depends on the atmospheric opacities and thus, directly on TWV. Because we have just one equation, we have to keep just one unknown term dependent on TWV. If one studies the behavior of $C(\tau_j, \tau_k)$ with increasing TWV, for values above 7 kg/m^2 the function varies very little. Because of this it can be approximated by a constant. In total we have the two focal point coordinates, the atmospheric parameters C_0 and C_1, and the slow varying function approximated by the constant $C(\tau_j, \tau_k) \approx 1.1$. The four parameters are determined through regression by using simulated brightness temperatures and atmospheric data from radiosonde profiles.

The stated weakness of the extended algorithm is its sensitivity to changes in the reflectivity ratio. In other words, for sea ice surfaces where the surface emissivity is a big distance away from the regression line used to calculate the ratio, the retrieval error can be as high as 3 kg/m^2.

2.8 Arctic algorithm synthesis

Because of the necessity of using a different channel coupling for different retrieval intervals, different retrieval equations and different calibration parameters for each pairing, the final algorithm has a modular structure, with three sub-algorithms that are used depending on the retrieval conditions.

The algorithm for low-TWV uses AMSU-B channels 20, 19, and 18 for the retrieval range 0 1.5 kg/m. These are the band channels around the strong water vapor line at 183.31GHz, and have the best accuracy and present the lowest error because the surface emissivity is indeed almost identical for all three frequencies.

The mid-TWV algorithm using AMSU-B channels 17, 20, and 19 takes over retrieval up to 7 kg/m. It is independent of surface but can encounter problems when approaching the retrieval limit. The assumption of equal emissivity is in use, even though there should be some differences because of the use of the 150GHz channel. Because of this difference in real surface emissivity a positive bias of up to 0.5 kg/m is possible [11].

The extended-TWV algorithm uses the channels 16, 17, and 20 and is responsible for the range 7 15 kg/m. The retrieval is restricted to sea ice regions and because of the simplified treatment of the surface emissivity difference; the error can reach 3 kg/m.

Because of the specific channel triplet used by each sub-algorithm, the set of four calibration parameters has to be determined for the L (low TWV), M (mid-TWV) and X (extended-TWV) cases.

2.9 How the retrieval works

The algorithm begins by using the full set of five brightness temperatures measured on all channels of the AMSU-B instrument. A first pass identifies pixels where the conditions $T_{(b,19)} - T_{(b,18)} < F^L_{19,18}$,$T_{(b,20)} - T_{(b,19)} < F^L_{20,19}$ hold true. For these pixels the low-TWV algorithm is applied.

If the first condition fails, the second one is checked: $T_{(b,20)} - T_{(b,19)} < F^M_{20,19}$, and $T_{(b,17)} - T_{(b,20)} < F^M_{17,20}$. Where this is true the mid-TWV algorithm is applied.

For applying the extended-TWV algorithm, the remaining pixels are tested for $T_{(b,17)} - T_{(b,20)} < F^X_{17,20}$ and $T_{(b,16)} - T_{(b,17)} < F^X_{16,17}$, and where true, processed. In addition to this test for channel saturation, the data is also classified for its surface type, and only sea ice areas are kept. This surface classification is done by a comparison with sea ice charts derived from SSM/I or AMSR-E data depending on the retrieval date.

Chapter 3

Retrieval over open ocean

The Melsheimer, Heygster algorithm represented the starting point of this project. The final goal was to retrieve water vapor in the Arctic region for the maximum range possible and over all surface types including open ocean. To this end two possible avenues were identified. Because microwave radiometer retrieval over open ocean is already an established method and accurate, validated retrieval sources can be found, a coupling with another source that could cover ice free water would offer a better coverage of the Arctic region. The other option would have been to attempt a modification of the extended sub-algorithm to enable it to work over open water. The key point of the previous extension was including surface emissivity information for the 89 and 150 GHz channels in the retrieval. This emissivity information was approximated into the constant reflectivity ratio. This ratio is only valid over ice surfaces and therefore obtaining such a constant for open water would enable a separate retrieval sub-algorithm for the ice-free ocean. A linear relationship between surface emissivities at the two frequencies would allow the approximation we need.

3.1 Comparing with a complementary source

Water vapor retrieval over open ocean is already available in the form of processed products from a number of sources so that we opted to proceed along the first path by finding a compatible open water retrieval which we could merge with the classic AMSU-B water vapor retrieval.

The AMSR-E water vapor product uses the water vapor absorption line at 22 GHz and is retrieved globally over oceans [24]. Because this product has such a large applicability it might deliver lower quality results for the polar areas were the proximity of sea ice, and the low sensitivity of the sensor to small water vapor values pose accuracy issues. The choice of the AMSR-E water vapor product is justified because all other comparable sources are more or less equivalent (e.g. Special Sensor Microwave/Imager - SSM/I or the Special Sensor Microwave Imager / Sounder SSMI/S), all using the same channel structure and providing results in the same range. Moreover this retrieval source is a proven method which has been validated against radiosonde data and provides good cover of the open water regions in the Arctic.

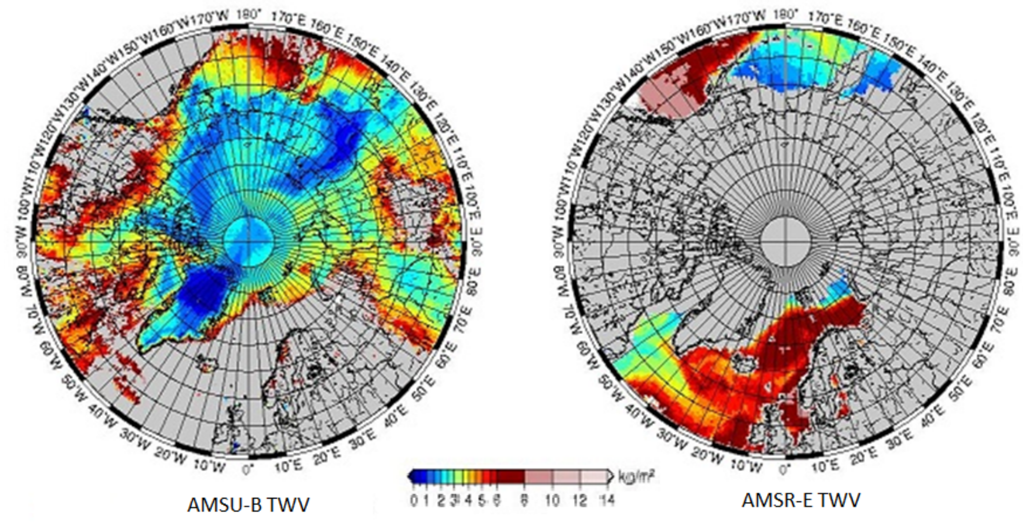

Figure 3.1: (a) on January 1, 2007. (b) The AMSR-E water vapor product is restricted to areas of open ocean .

A typical comparison of the retrieved TWV from the AMSU-B extended algorithm and AMSR-E water vapor product is shown in Figure 3.1. In order to merge the two products on a common grid we wanted to know if there is any overlap in coverage. Because the AMSR-E retrieval algorithm rejects pixels located in proximity to sea ice or landmasses the only overlap would be possible if the AMSU-B retrieval encounters water vapor values below 6 kg/m^2 so that the mid-TWV sub-algorithm can be applied above open ocean.

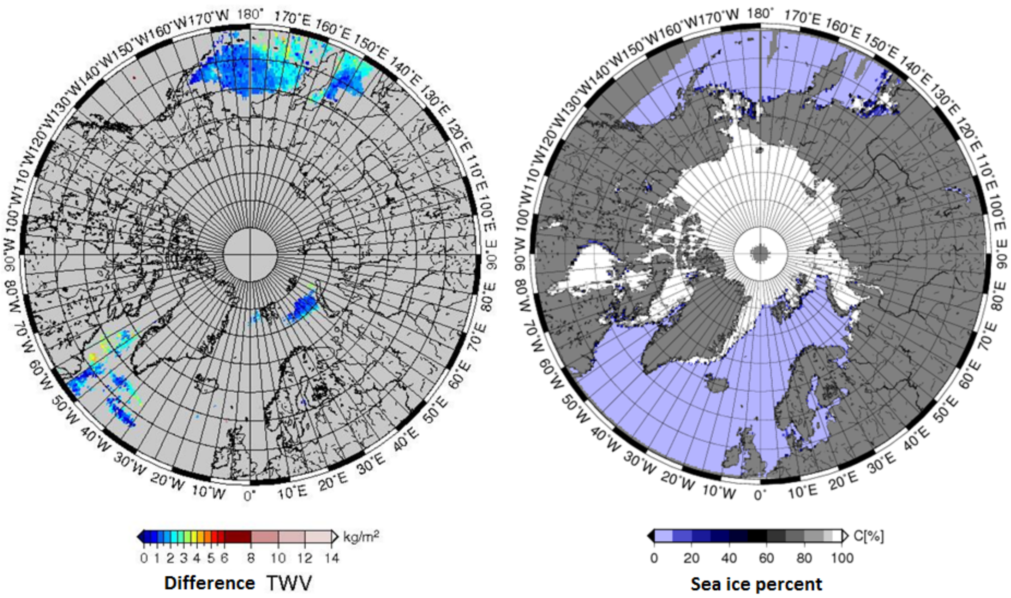

Figure 3.2: Difference map (a) AMSU-B - AMSR-E retrieval.(b) Sea ice map. January 1, 2007.

The difference map in Figure 3.2 shows the overlap that can normally happen between AMSU-B retrieval and AMSR-E water vapor product during the drier part of the year. If the atmospheric total water vapor load is low enough (¡6 kg/m^2), the AMSU-B retrieval can reach as far south as the 50th parallel. When compared with the sea ice extent of the same day, all overlap is shown to appear above ice-free ocean as expected. The map in Figure 3.2 a) shows a constant positive difference for the AMSU-B retrieval which ranges from below 1 kg/m^2 in the northernmost regions of overlap and tends to rise up to 4 kg/m^2 in the lower latitudes.

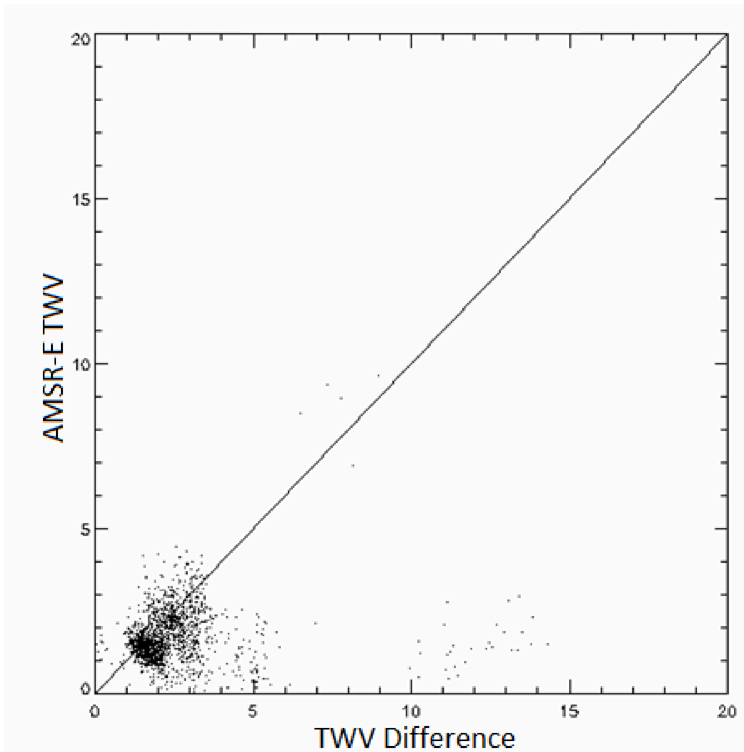

Figure 3.3: Difference values vs TWV values from the AMSR-E retrieval scatter for 1st January 2007

When comparing the two retrieval products it became apparent that various patterns can be identified in the AMSU-B retrieval data depending on local conditions of sea ice cover, atmospheric water vapor load or land-mass presence. To ensure the widest coverage for the AMSU-B product, most of the comparisons were done for winter months, when the cold polar atmosphere is less moist. In the summer months the atmospheric water vapor load is on average so high that the area where the AMSU-B algorithm can retrieve data is too small to observe any overlap. Three areas were chosen that best exhibit these patterns: the northern part of the Barents Sea, the region of the Kamchatka Peninsula and the Bering Sea.

3.1.1 Barents Sea

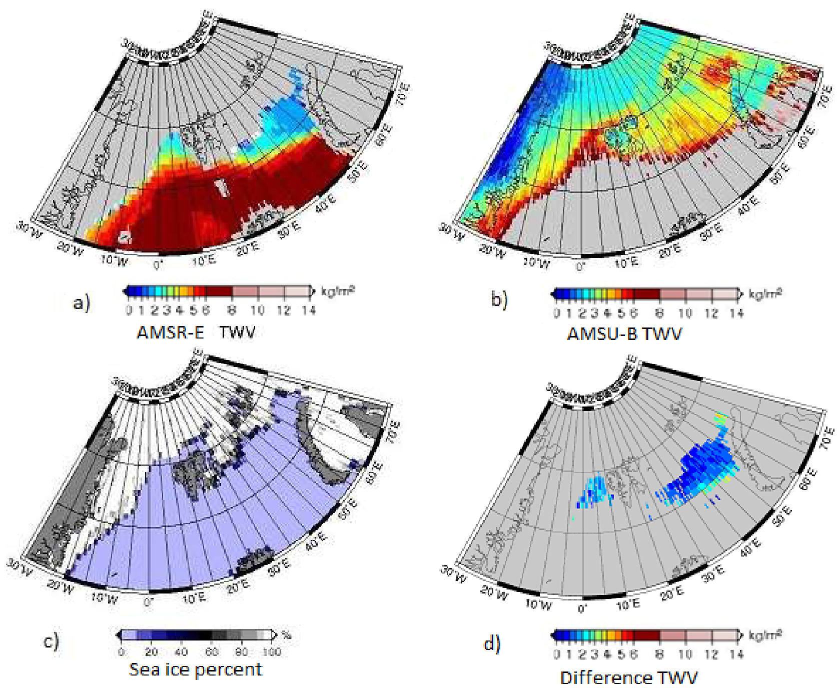

Figure 3.4: Barents sea area 1st January, 2007 (a) AMSR-E TWV retrieval over open ocean. (b) AMSU-B retrieval. (c) Sea ice map obtained from AMSR-E data . (d) Difference map

In this region the AMSU retrieval provides high TWV values for areas around the Svalbard islands. On the sea ice map it is clearly seen that, except for a small area in the north-eastern part, the coast of the Svalbard islands is ice free, as is the western shore of Novaya Zemlya. In particularly visible on the western coast is the abrupt jump in values in the AMSU-B data from 2-3 kg/m^2 above the island itself and the ice covered eastern shore to 4-5 kg/m^2 as the retrieval encounters open ocean. While it is normal that the atmospheric water vapor load should increase above open ocean because of the direct effect of evaporation, this jump in value is interesting in relation to the values the AMSR-E product reports for the same regions. In the distribution of retrieval differences between the AMSU-B and the AMSR-E products, no obvious trend can be established as the overlap areas are relatively small. One observable feature is that the AMSU-B product has a positive bias varying between 1.5 and 3 kg/m^2 over the AMSR-E retrieval.

3.1.2 Bering Sea

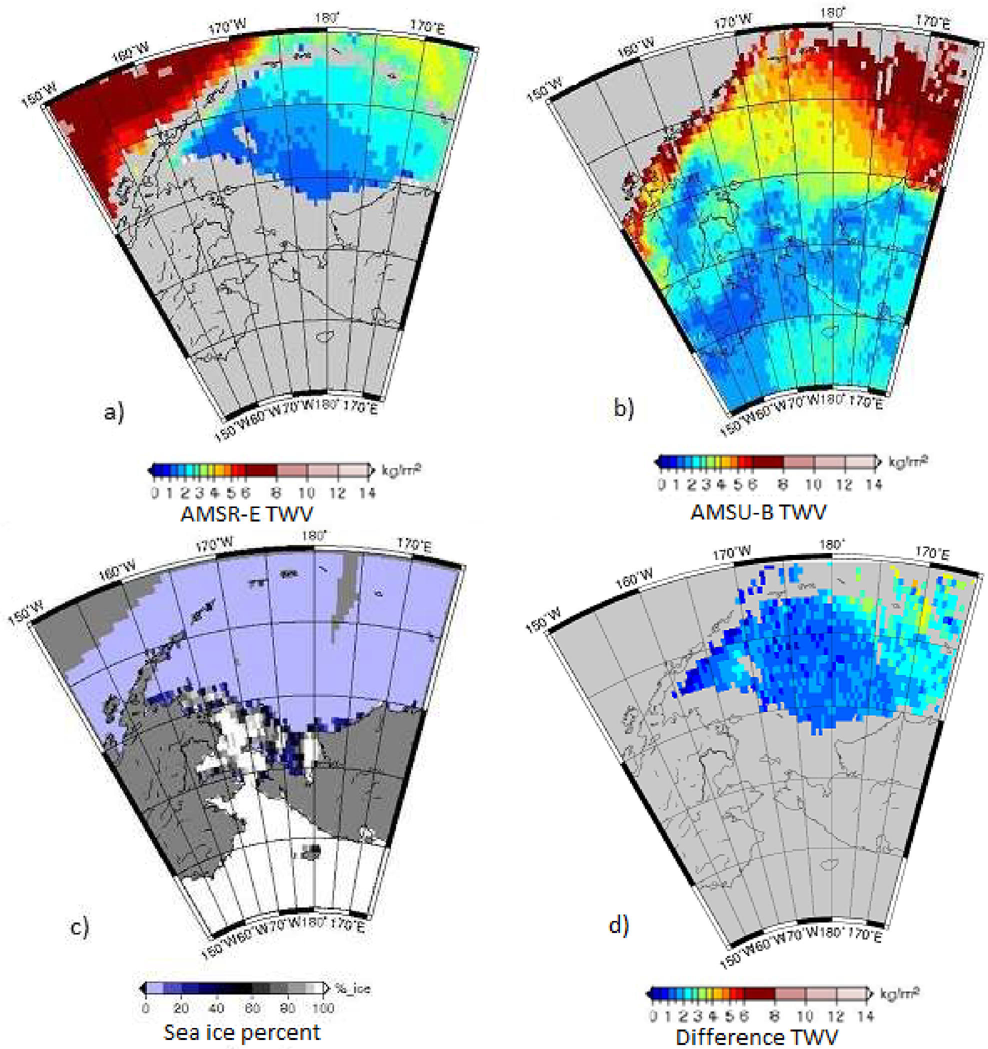

Figure 3.5: Bering sea area 1st January, 2007 (a)AMSR-E TWV retrieval over open ocean . (b) AMSU-B retrieval . (c)Sea ice map . (d) Difference map.

The Bering Sea region represents the best example of an ice free area over which the algorithm retrieves anomalously high TWV values. When comparing the data from the two instruments, although TWV values in adjacent areas (above water for AMSR-E, and above sea ice for AMSU-B) are comparably low, as soon as the AMSU-B retrieval encounters open ocean the values peak sharply (from 1.5- 2 to 3.5-4 kg/m^2). In the difference map for this region it is more obvious that the differences increase as the retrievals encounter higher water vapor load towards the upper right corner of the image.

3.1.3 Kamchatka Peninsula

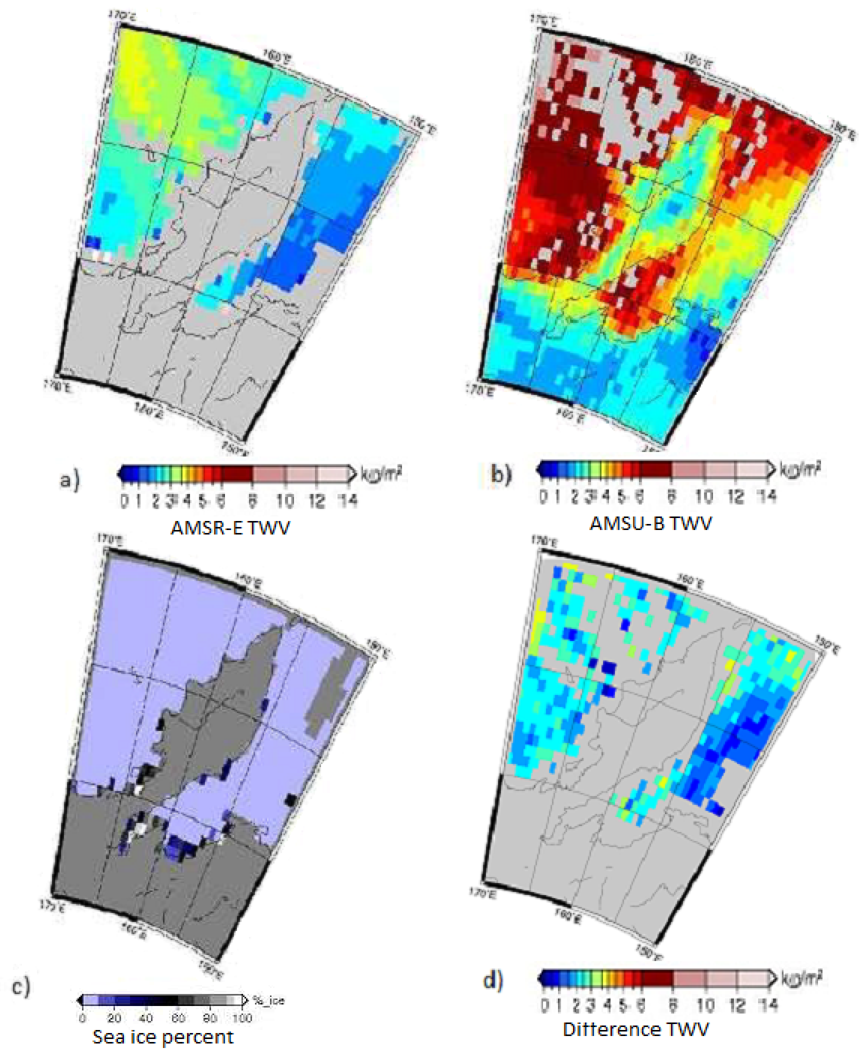

Figure 3.6: Kamchatka area 1st January 2007 (a) AMSR-E TWV retrieval over open ocean .(b) AMSU-B retrieval .(c) Sea ice map .(d)Difference map

The sea around the Kamchatka Peninsula contained little if any sea ice during the polar winter of 2007, and when compared to the AMSR-E retrieval, the Melsheimer - Heygster algorithm reports values up to two times greater than the former throughout the entire open ocean area. The cause for this inaccuracy is still not fully understood as the TWV content is not high enough to require surface emissivity information. Again, AMSU-B values above land surfaces contrast sharply with the adjacent open ocean areas while they are in accordance with AMSR-E ocean data. Comparable 1.5-3.5 kg/m^2 range retrieved by AMSU-B above land mass and AMSR-E retrieved for neighboring ocean are in contrast with the high 5-7 kg/m^2 retrieved by AMSU-B over open water.

3.1.4 Behavior in the overlap zone

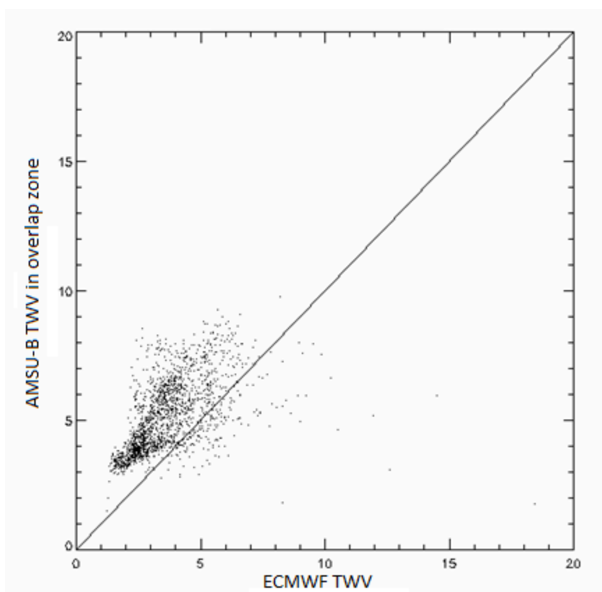

Figure 3.7: Behaviour of the AMSU-B retrieval in the overlap area when compared to ECMWF model data 1st January 2007.

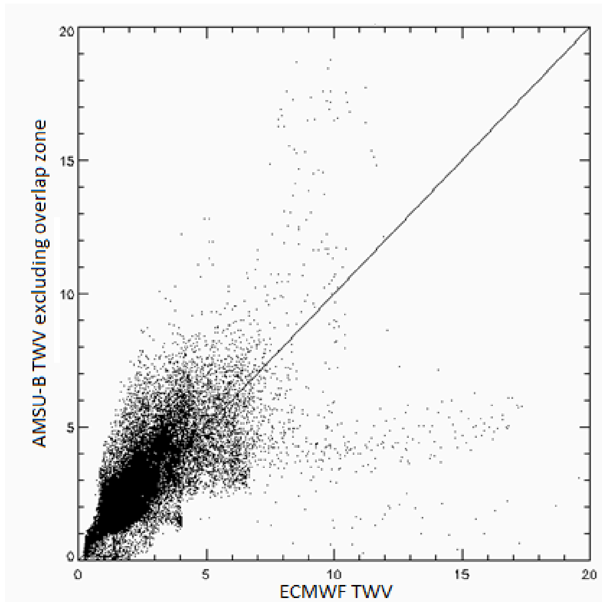

Figure 3.8: Scatter plot of ECMWF model data and AMSU-B water vapor retrieval without the overlap areas 1st January 2007.

The scatter plot in Figure 3.7 shows the behavior of the AMSU-B retrieval in the overlap areas shown in Figure 3.2 when matched with ECMWF model data for those regions. The constant bias of AMSU-B retrieval is shown in comparison with the identity line. All data points are above the 1.5 kg limit of the low-TWV algorithm and therefore represent only mid-TWV retrieval over open ocean. For most points the bias is positive with differences of 2-4 kg/m^2 from the model but there are also a few outliers where the AMSU-B algorithm underestimates TWV values by more than half.

For the central Arctic region, most TWV values are below 5 kg/m^2 and the AMSU-B retrieval is in agreement with ECMWF model data. In the mid-TWV value range (2-6 kg/m^2) the scatter increases but the grouping is closer to the identity line than for retrieval over open ocean. There are also few outliers for the higher values of water vapor that can be attributed to the reduced accuracy of the extended algorithm.

In Appendix A the behavior of AMSU-B retrieval in the overlap areas is illustrated. The maps show the differences between the AMSU-B and AMSR-E retrieval. The difference values are generally small, but for a few locations in the lowest latitudes. In general, TWV values tend to increase with decreasing latitude because of the more active atmospheric circulation that can bring moist air in the area. Also, increasing air temperatures in the lower latitudes mean more evaporation from the ocean surface. The most interesting feature of these maps though, is that for the whole range of six days the Melsheimer-Heygster algorithm overestimates water vapor values over most of the overlap areas when compared to the AMSR-E TWV product. This comparison can give no definite conclusion over which method is actually right, as these regions represent weak points for both retrieval methods. The AMSU-B retrieval will assume the same surface emissivity for all channels even though this might not be the case for open ocean surfaces. At the same time, the AMSR-E algorithm is not specialised for such low TWV values and, consequently the retrieval error represents an issue [22]

3.2 Composite maps

As mentioned above, the AMSU-B and AMSR-E retrievals of atmospheric water vapor content are complementary in that, together they provide a good cover for the whole Arctic region. Because of this, we combined the retrieval products of the two instruments into one composite map that covers the entire area. The AMSR-E based retrieval is set to have priority over the AMSU-B data wherever they overlap (above open ocean) so as to avoid the uncertain behavior of the AMSU-B retrieval over the ice free ocean.

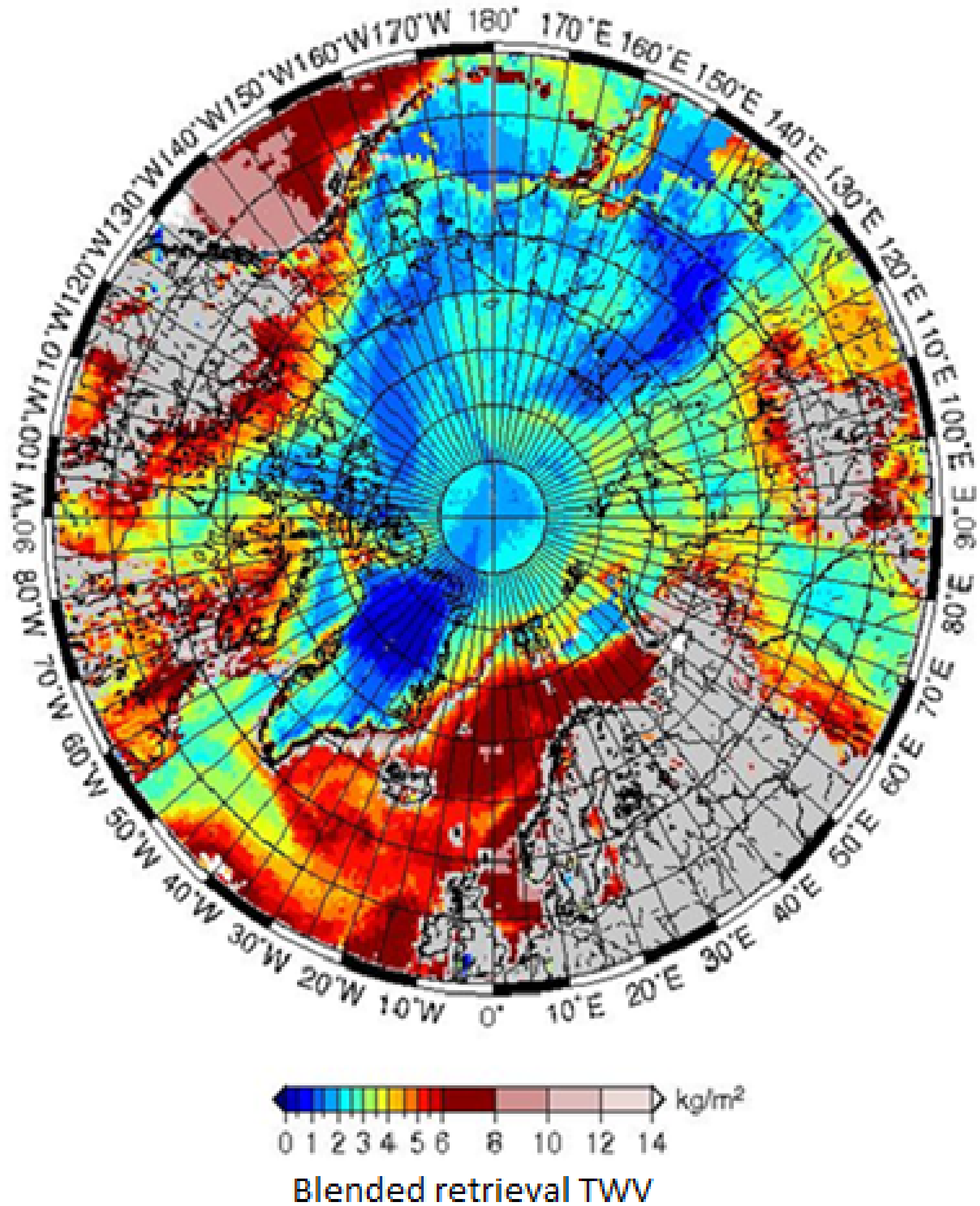

Figure 3.9: Composite map made by gridding on the same map retrieval values from the AMSU-B and AMSR-E sources, 1st January, 2007.

As expected, the composite map presents the high values retrieved by the AMSU-B algorithm in the border areas, where the ice cover stops and the open ocean starts. As shown above, the Melsheimer-Heygster algorithm retrieval values tend to peak as the surface changes from sea ice to open ocean, and while eliminating the areas of inaccurately high values above the ocean, the jump in values is still evident at the edge of the ice. This could be explained through the fact that, because of the instrument resolution, individual pixels would actually contain parts of sea ice and open water, thus influencing the accuracy of the retrieval. This behavior is translated into a ridge of high values near the water-ice boundary is on the map. In trying to clean up these problematic areas, we used sea ice concentration data in order to further constrain the Melsheimer-Heygster algorithm retrieval. By removing pixels from areas with sea ice content below 95%, the high value ridges coming from the mid-TWV algorithm could be deleted. The direct result of this approach is that we now have a blank band between the AMSU-B retrieval results and the AMSR-E data where the ridges used to be Figure 3.10.

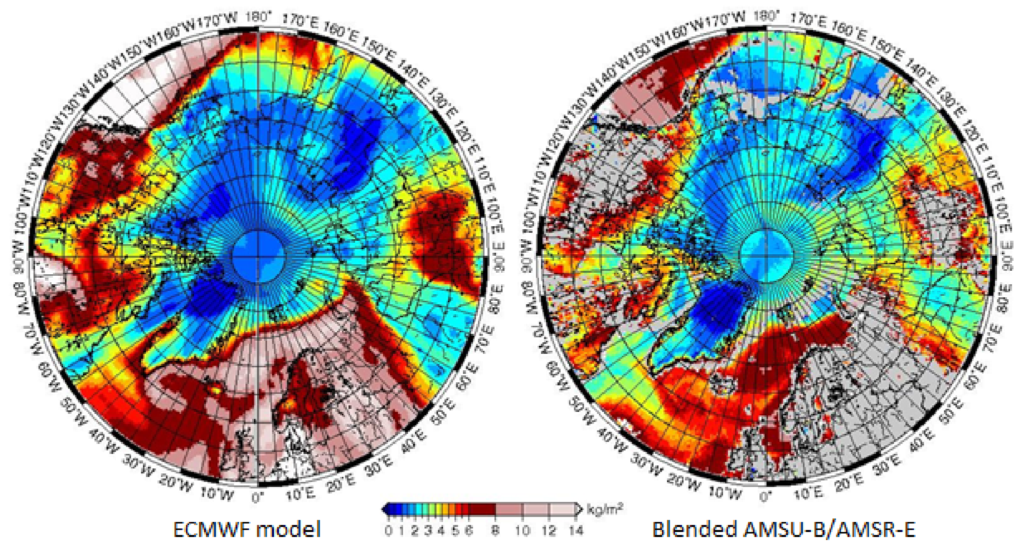

Figure 3.10: Composite map with a more restricted range of retrieval for the AMSU-B algorithm compared to ECMWF model data for 1st January, 2007

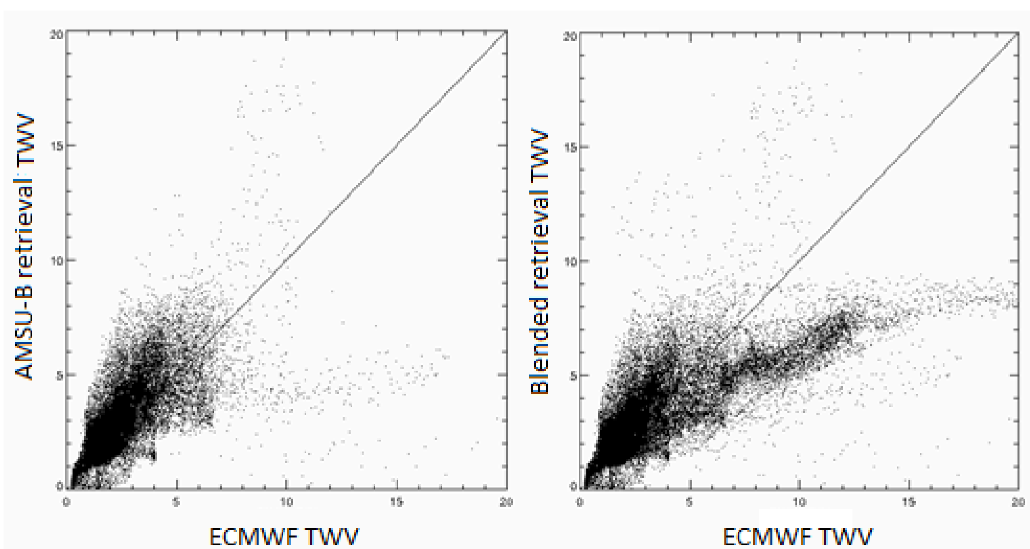

Figure 3.11: Scatter plots for AMSU-B original retrieval vs EMCWF (left) model and AMSU-B + AMSR-E blended retrieval vs ECMWF (right)

In Figure 3.11 it is obvious that adding the AMSR-E pixels to the final product improves the coverage but because of the lower accuracy of the AMSR-E retrieval the overall product correlation with ECMWF model data is lowered.

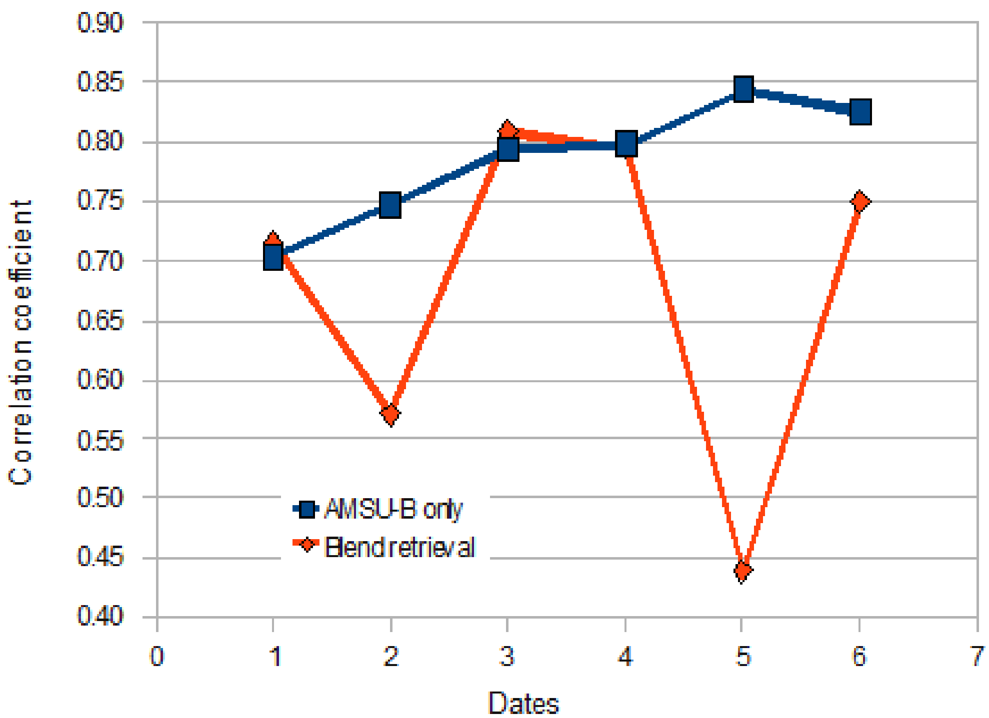

Figure 3.12: Correlation comparison for blended TWV product and original AMSU-B retrieval. Time scale is 1st-6th January 2007

To roughly compare the performance of the original AMSU-B retrieval with the product obtained from blending it with AMSR-E retrieval over ice-free oceans, we looked at the correlation between each retrieval product and ECMWF model data. The results are shown in 3.12. The blended product can at most match the correlation of the AMSU-B product, while often going below it. The coverage provided is obviously better then for the

AMSU-B retrieval alone, but because a good match in synchronisation cannot be guaranteed for the two instruments (different overflight characteristics), and the error of the AMSR-E product for the Arctic region conditions [22], the blended product represents a downgrade in the retrieval quality and not an improvement.

3.3 Modifying the extended algorithm

Considering the drawbacks of the blending approach, we concluded that the goal of achieving overall coverage of the Arctic region with the best accuracy possible would be better served by attempting to further extend the original Melsheimer -Heygster algorithm to include retrieval over open ocean.

In order to determine the feasibility of this option we needed to find out if a suitable linear relationship exists between surface emissivity in the two outermost retrieval channels at 150 and 89 GHz. A stable linear dependence would allow us to use the same technique as for the first extension of the algorithm for sea ice. By using the same retrieval equation and replacing the calibration coefficients and the ratio of reflectivities, a separate module for retrieving water vapor in the extended range only over open water could be implemented.

3.4 Ocean surface emissivity simulations

The ocean emissivity model FASTEM takes into account several parameters. Besides the characteristics of the AMSU-B instrument, very important are the sea surface temperature and roughness. The simulations were run for sea surface temperatures between 0 and 6 ^{o}C, which are what one might expect for the Arctic Ocean, in increments of 2 ^{o}C. The other parameter that would determine a strong variation in surface emissivity is the ocean surface roughness. Wind speed is the determining factor for surface roughness, and within certain ranges surface emissivity will be directly proportional to the wind speed. In Figure 3.5 we can see the behavior of the ocean surface emissivities for the five channel frequencies of the AMSU-B instrument. Because the three band channels around 183.3 GHz are so close to each other, the corresponding emissivities are almost identical and thus represented by only one curve on the graph. Important to note is the big difference between the curve for 89 and the one for 150 GHz, which illustrates why the assumption of equal emissivities cannot be sustained for this pair of channels. Also interesting is the difference between the 183 and 150 GHz frequencies which would explain the positive bias of water vapor retrievals above open ocean under the assumption of equal emissivity.

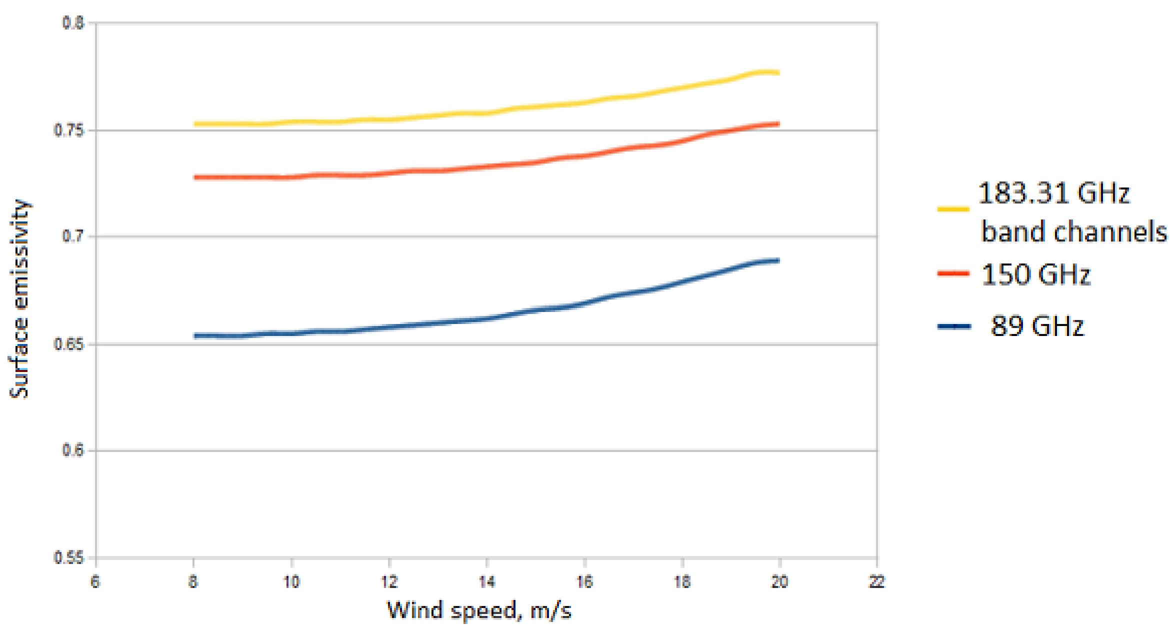

Figure 3.13: Surface emissivities' dependence on wind speed

From Figure 3.13 it is clear that all frequencies, the surface emissivity increases with wind speed. Because of the smooth linear dependence between the two values, a constant ratio for reflectivities at the two channels can be obtained following the same method as for the extended algorithm.

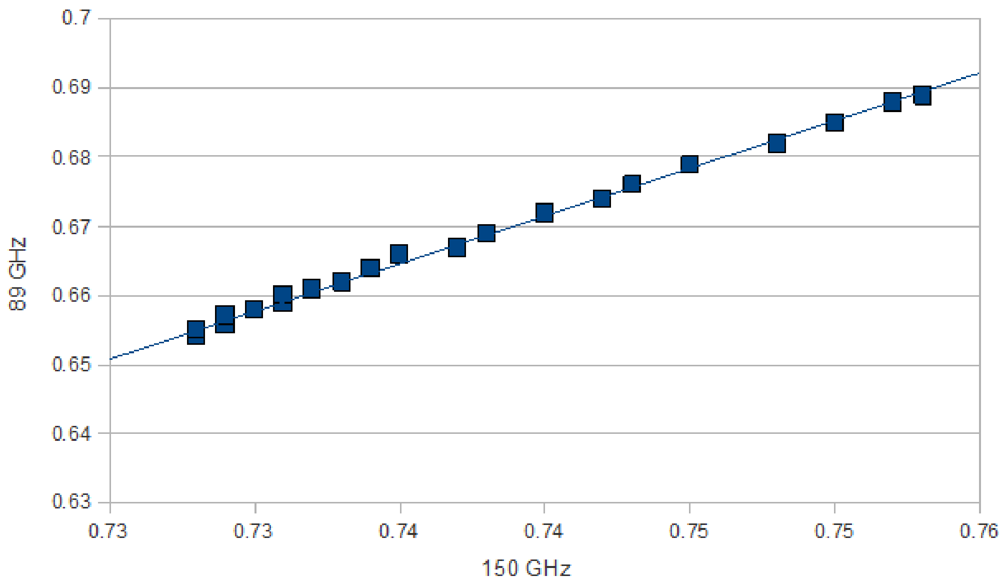

Figure 3.14: Relationship between surface emissivity at 89 and 150 GHz

Following the method described in [10] we drew a regression line for ocean surface emissivity at 150 and 89 GHz (Figure 3.14) and we found the following linear relationship:

$$\epsilon_{89} = 1.38 \cdot \epsilon_{150} - 0.35$$

In the case of sea ice emissivity studied in the original algorithm, the constraint that $\epsilon_{89}(\epsilon_{150} = 1) \approx 1$, had to be imposed on the system in order to express the ratio of reflectivities as a constant of the form shown in (20), independent of variable surface emissivity.

From this regression equation we get the ratio of reflectivities: $\frac{r_150}{r_89} = 0.79$. Using this relationship the calibration parameters C_0 and C_1 were also determined from the regression fit as described in Section 2.4.

3.5 Retrieval with the modified algorithm

The open ocean retrieval needs a different set of calibration parameters and a modified retrieval equation that uses the reflectivities ratio for ocean surface. This new retrieval product should add information about ocean surfaces. In the cold months of the year, water vapor load over the oceans is low enough to be retrieved by the mid-TWV and extended algorithms (2-14 kg/m^2). Because in the comparisons with the AMSR-E water vapor product it became clear that the mid-TWV retrieval over open ocean was unreliable, only the modified extended algorithm was used. The practical interval where the mid-TWV algorithm could have worked above oceans was between 4.5 6 kg/m^2, so that the gaps that occur because of filtering this out are small.

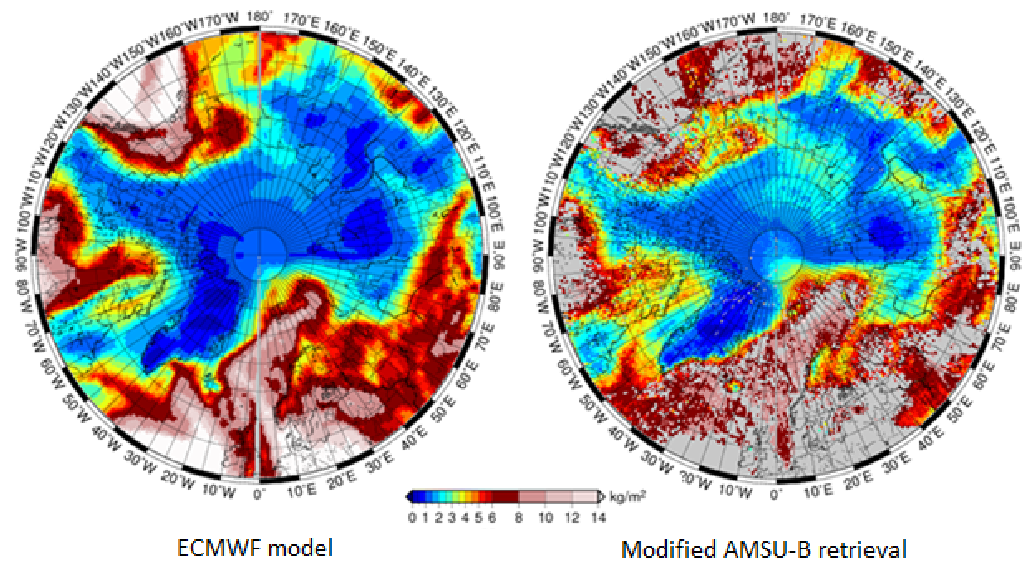

Figure 3.15: ECMWF model data (left). New AMSU-B retrieval including open ocean (right). 6th March 2009

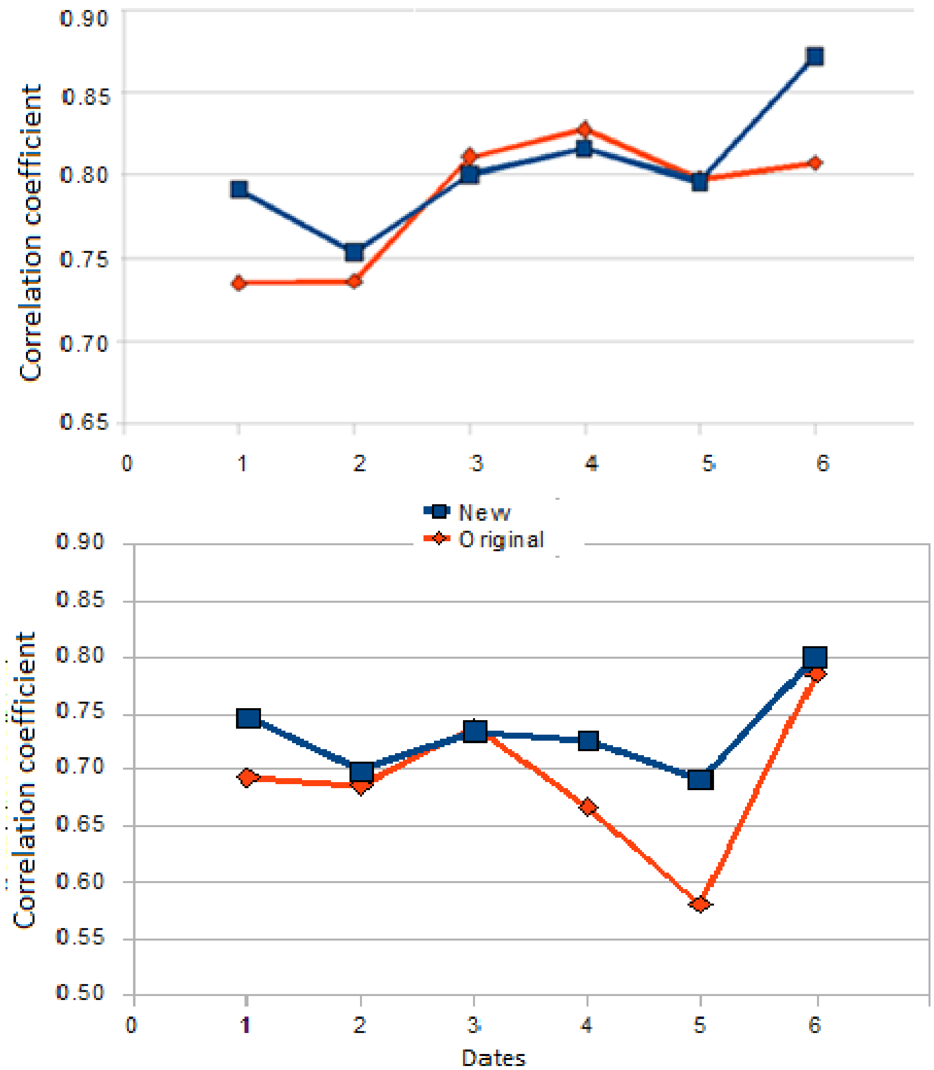

Figure 3.16: Correlation comparison between the original AMSU-B retrieval and the new retrieval including information about open ocean surfaces for the time period 1st 6th March 2009 (upper image), and 1st-6th December 2009 (bottom image).Note that for the upper image the Y axis has been stretched slightly.

Figure 3.15 represents a fortunate scenario for the new extended algorithm because water vapor load above oceans between the possible retrieval ranges (6-14 kg/m^2) allowed a good retrieval yield that complemented the original retrieval and resulted in overall a better correlation with the corresponding ECMWF model in Figure 3.16

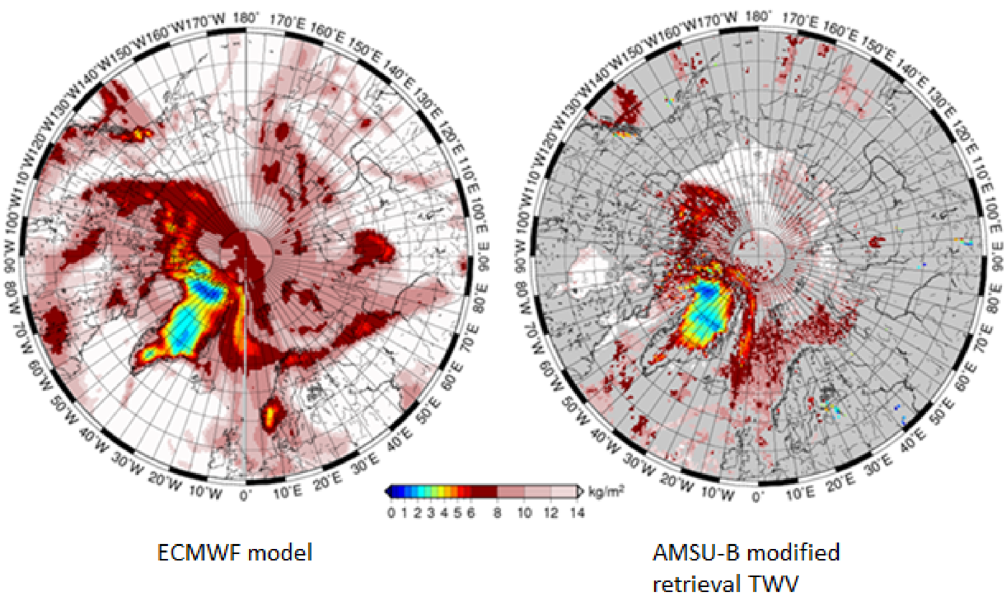

Figure 3.17: ECMWF model data (left). AMSU-B retrieval including ocean surfaces (right). 5th June 2009

After applying the new retrieval in the summer months, when the water vapor load above the Arctic is much higher (see Appendix B), the results are not as good. Because towards the upper limit of the retrieval range the error increases up to 3 kg/m^2, a product with pixels within this range is consequently less reliable. This is the case portrayed in Figure 3.16. were the algorithm retrieves TWV above a few areas of open ocean where the atmospheric load is low enough. When comparing the new retrieval and the original one, the correlation with ECMWF data is lower for the whole temporal range. This is shown in Figure 3.18. This performance of the modified algorithm can be argued as being an improvement over the original algorithm or not. While for the winter months, where the modified method ensures a larger coverage of the Arctic (see Appendix C.2) and a better correlation with the model, in the summer the situation is less clear cut. The modification allows the algorithm to see farther then before and include regions of open ocean from which there was no prior information (see Appendix C.1), but the quality of this data is uncertain because of the potential errors as high as 20% for the maximal retrieval value. This limitation of the algorithm cannot be overcome at the present because of the inherent hardware limitations of the retrieval instrument, but as there are few possible sources for TWV information in the Arctic, the ability to retrieve some information with high error where previously there was none is still a positive development.

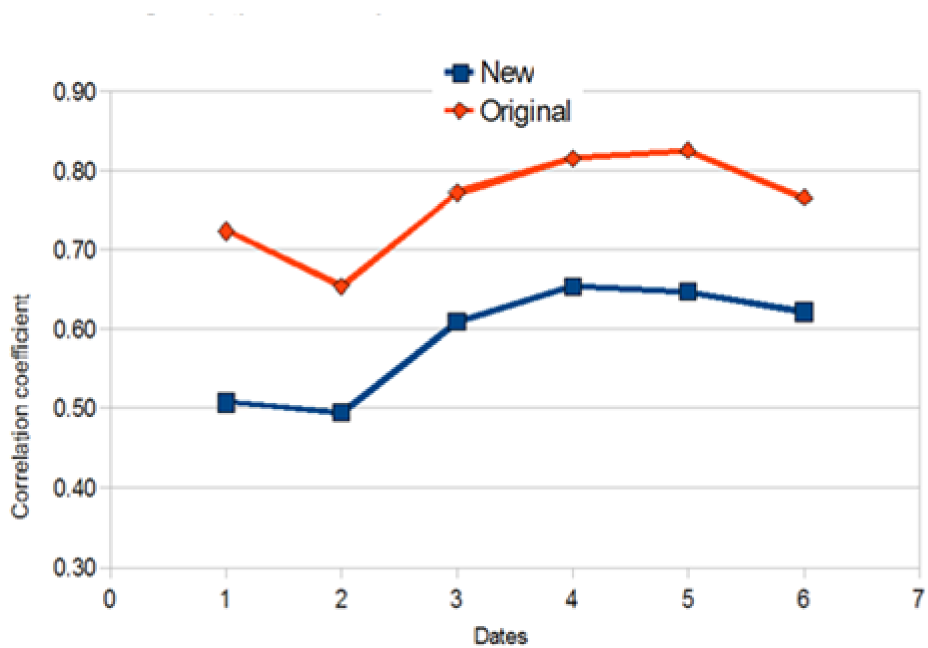

Figure 3.18: Correlation between AMSU-B retrievals and ECMEF model data for timespan 1st 6th June 2009. Correlation comparison between the new retrieval algorithm that includes open ocean surfaces and the original AMSU-B retrieval

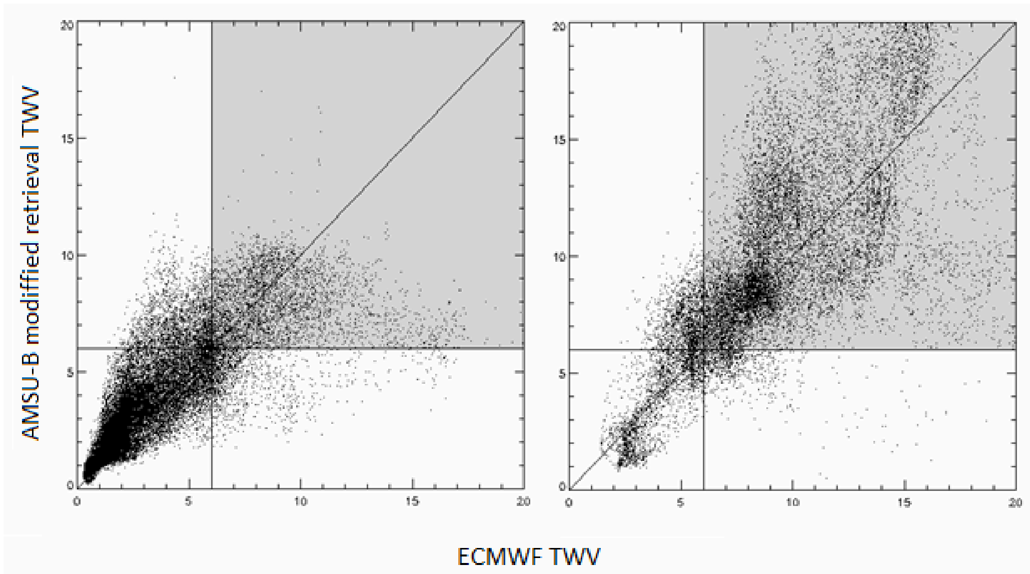

Figure 3.19: Scatter plots for the best retrieval case of 6th March 2009 (left) and the worst retrieval case for 2nd June 2009 (right), 55700 data points

The scatter plots in Figure 3.19 demonstrate the behavior of the new retrieval algorithm in the two cases of overall low water vapor load that is characteristic for the Arctic winter and the one with high atmospheric water vapor load that is the norm in the Arctic summer. For winter days there are a lot of low value pixels in the low TWV retrieval range which has the best accuracy. In the lower left square of each plot are the pixels corresponding to the low and mid-TWV retrieval algorithms while the upper right square surrounds pixels from the extended-TWV retrieval. For the Arctic winter months the threshold of 6 kg/m^2 is exceeded in relatively few cases and of these most remain below 10 kg/m^2. Judging just from the comparison with ECMWF data, for this water vapor range the extended algorithm can offer reliable retrieval over open oceans, thus constituting an improvement over the original algorithm. In the summer season there are no pixels with values below 2 kg/m^2, the bulk of the retrieval pixels are situated above the

6 kg/m^2 limit with a good portion around the 15 kg/m^2 value. This places the extended algorithm under strain because of the high water vapor load that is close to the saturation limit of the 183$\pm$7 GHz channel, thus resulting in retrieved values with higher error probability than at lower TWV ranges. The large number of pixels added by the extended retrieval over open ocean are strongly scattered, thus reducing the overall correlation with ECMWF model when compared to the original algorithm.

3.6 A potential extension for open ocean retrieval in the mid-TWV algorithm

In the comparison with the AMSR-E product it became evident that the mid-TWV algorithm had high errors when retrieving water vapor above ice-free ocean surfaces. Because of the surface emissivity difference at the 150 and 183$\pm$7 GHz channels that is not compensated in the original algorithm, the retrieval would always overestimate the water vapor load as seen in Figure 3.7. To address this problem we can follow a similar approach as the one used for modifying the extended-TWV algorithm. Using surface emissivity information at the required frequencies and using the retrieval equation from the extended-TWV algorithm a new subcomponent of the mid-TWV algorithm can be implemented. This component would retrieve water vapor in the 2-6 kg/m^2 value range load only above open ocean.

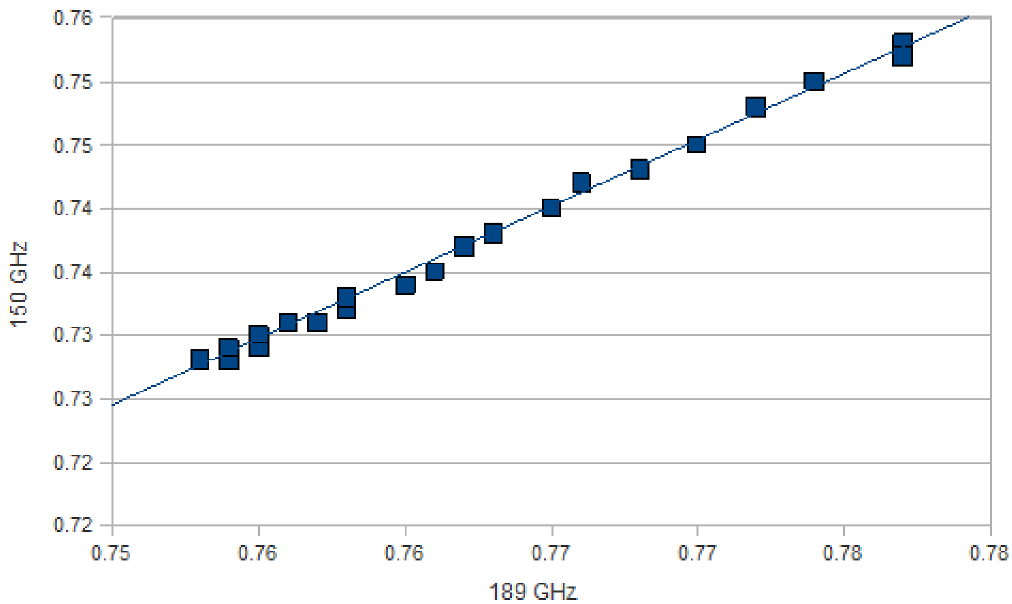

Figure 3.20: Regression plot for open ocean surface emissivity at 189 vs 150 GHz

Following the regression fit in Figure 3.20 we obtained a linear relationship for ocean surface emissivity at 150 and 183 GHz:

$$\epsilon_{150} = 1.04 \cdot \epsilon_{183} - 0.06$$

From which we get the ratio of reflectivities:

$$\frac{r_{183}}{r_{150}} = 0.89$$

In addition to the C_0 and C_1 parameters, the $C(\tau_j, \tau_k)$ function, that is dependent on the atmospheric opacity is necessary for a retrieval when different surface emissivity is considered (see Section 2.7). This function depends directly on TWV and it has been shown that for the 89 and 150 GHz frequencies, above 7 kg/m^2 water vapor load it is almost constant. If we would attempt to modify the mid-TWV algorithm, the $C(\tau_j, \tau_k)$ has to be included into the new retrieval equation and calculated for the 183±7 and the 150 GHz channels.

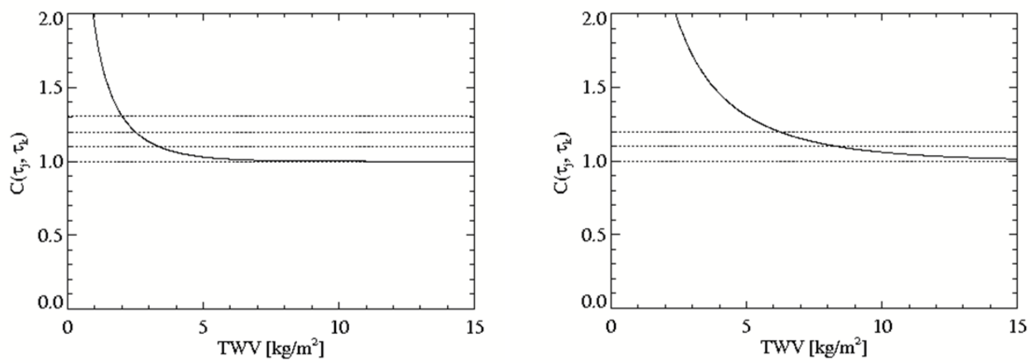

Figure 3.21: $C(\tau_j, \tau_k))$ parameter for extended-TWV algorithm (right) and for mid-TWV algorithm (left)

For the mid-TWV channels, the $C(\tau_j, \tau_k)$ function behaves slightly different than for the extended-TWV coupling. Within the 2-6 kg/m^2 interval it drops rapidly from 1.4 down to 1.0 but as it has been found that changes on the order of 0.2 in $C(\tau_j, \tau_k)$ lead to differences in the third significant digit of the C_0 and C_1 parameters, even this increased variability might not pose a problem. Further investigation into modifying the mid-TWV algorithm was not pursued but it is considered to be a viable option for further improvement of the Arctic retrieval algorithm.

Appendix A

Retrieval behavior in the overlap zones

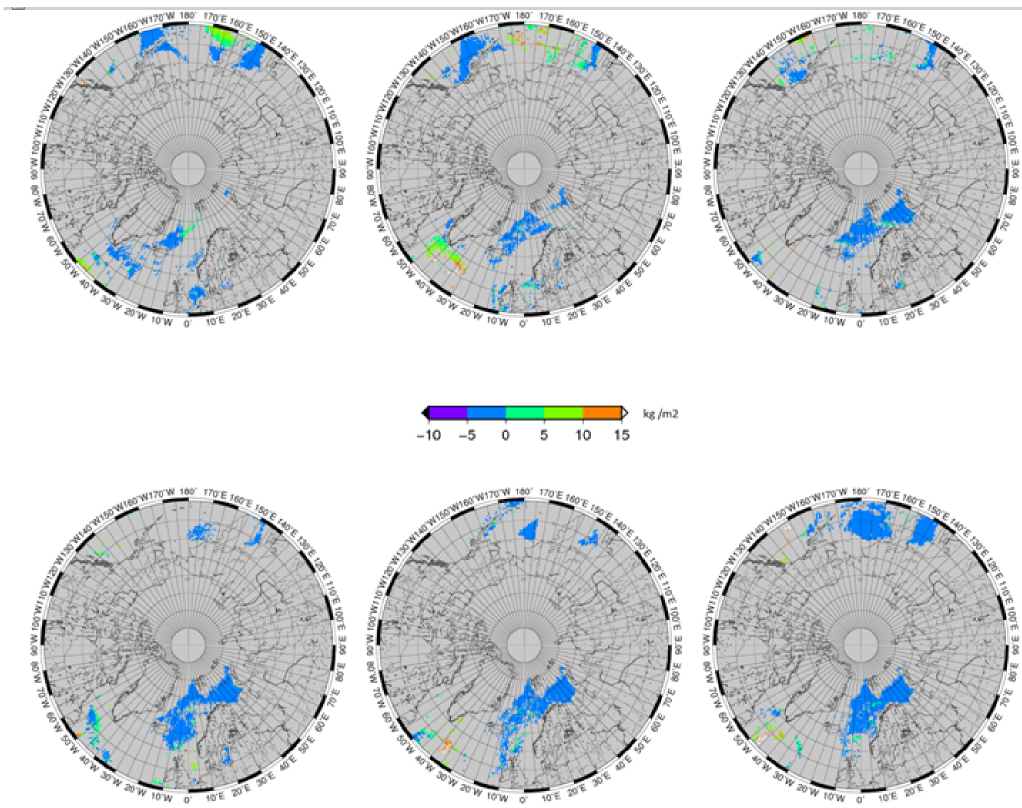

Figure A.1: AMSR-E minus AMSU-B retrieval without taking the absolute value. The negative values indicate the positive bias of the AMSU-B algorithm over open ocean areas. Timespan is 1st(upper left) to 6th (lower right) January 2007

Appendix B

Original AMSU-B retrieval in the summer season

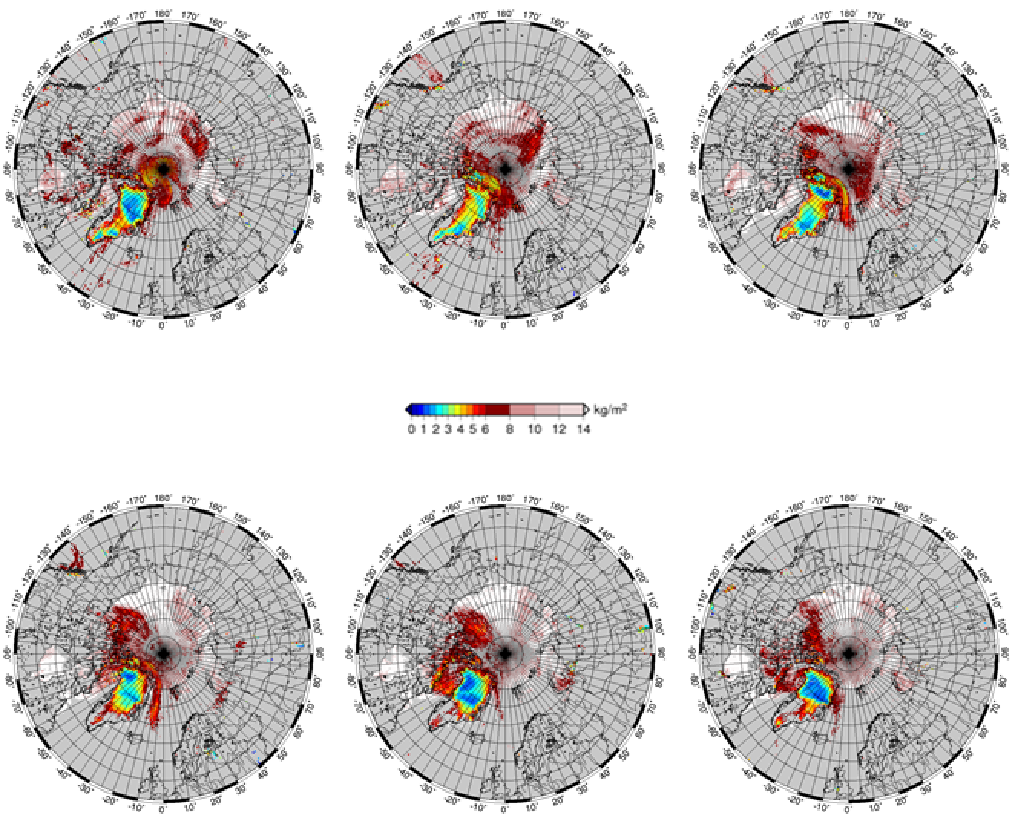

Figure B.1: A typical retrieval product of the original AMSU-B algorithm in the Arctic summer season. Because of the very high water vapor load characteristic of this period, the area retrieved by the original algorithm is significantly reduced when compared with the winter season. Timespan is 1st(upper left) to 6th (lower right) June 2009

Appendix C

New retrieval including open ocean areas

C.1 Summer retrieval

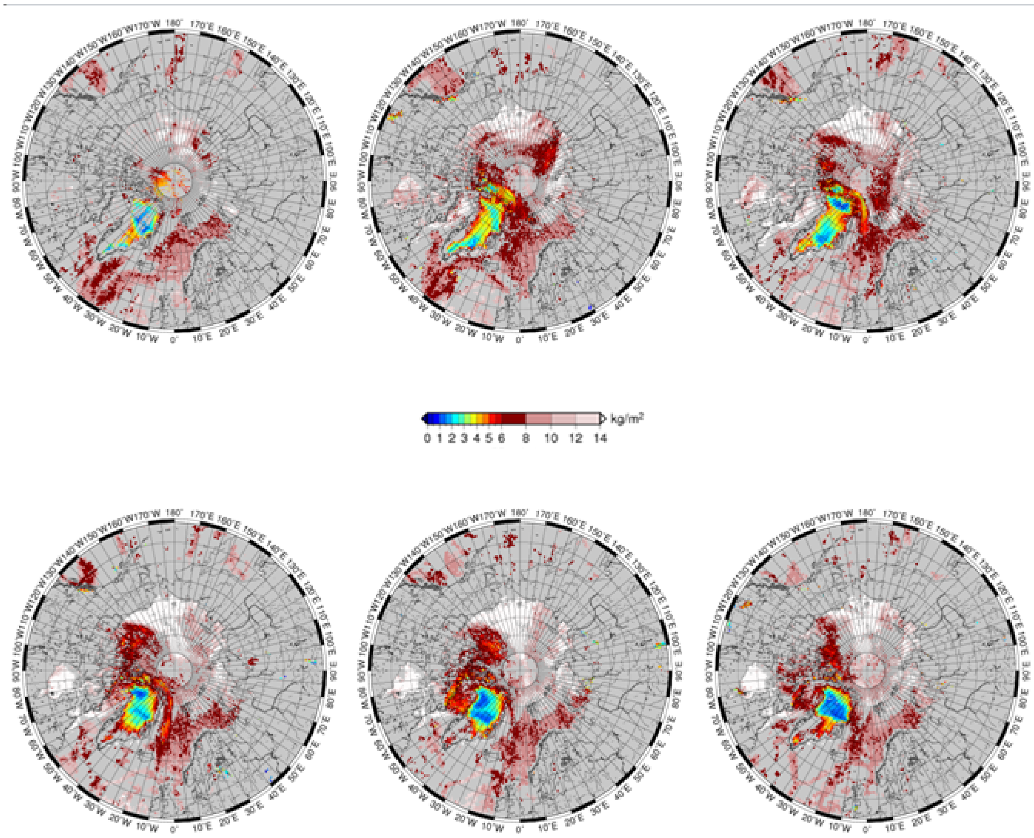

Figure C.1: Retrieval using the modified extended algorithm that includes open ocean regions. Timespan is 1st(upper left) to 6th (lower right) June 2009

C.2 Winter retrieval

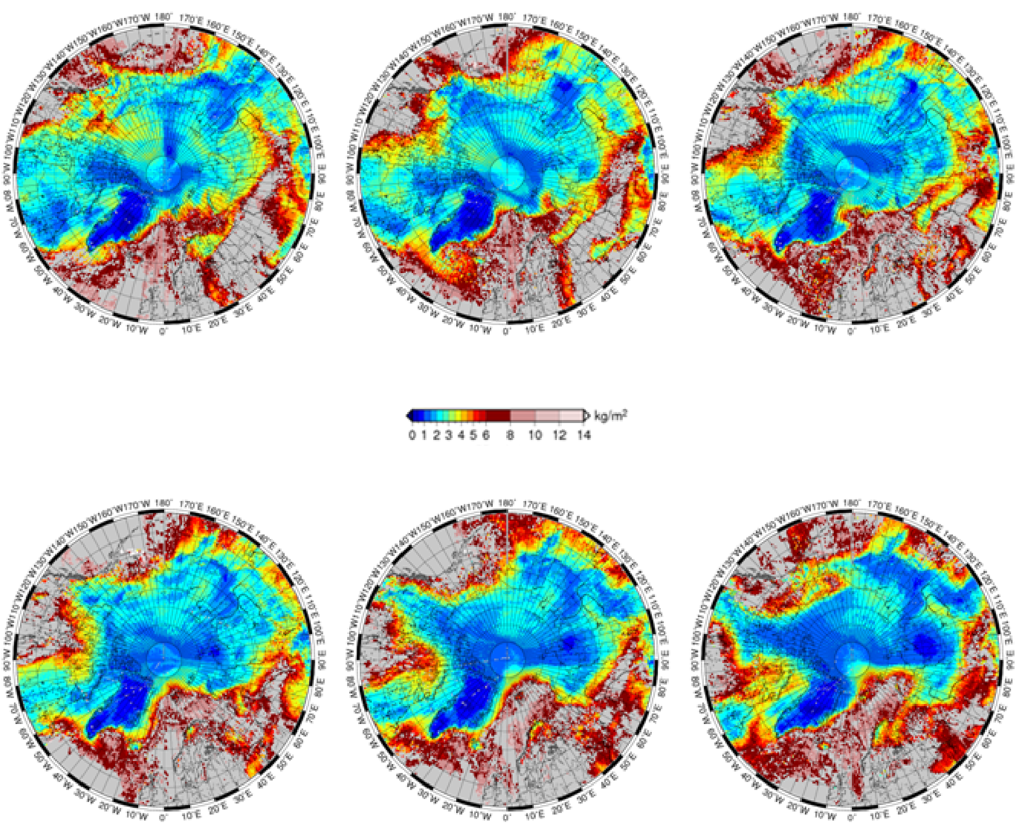

Figure C.2: Retrieval example for the Arctic winter season. This week coincided with the sea ice maximum in the Arctic, usually an event correlated with very low atmospheric water vapor load. Timespan is 1st(upper left) to 6th (lower right) March 2009

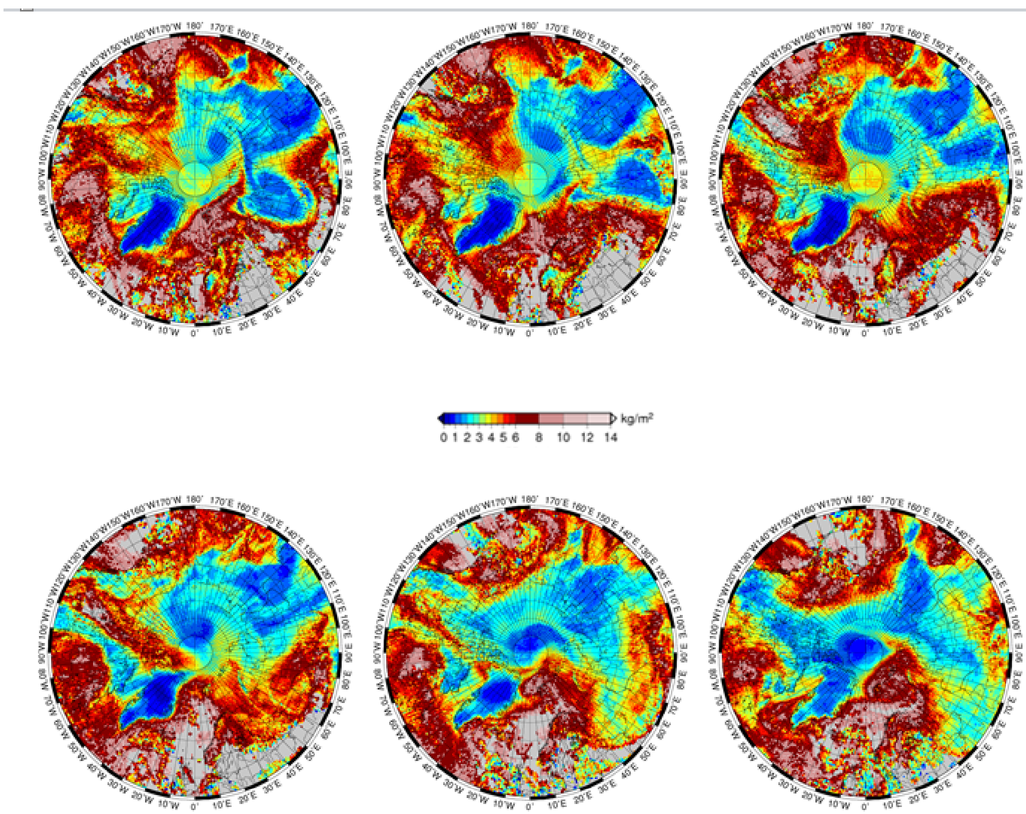

Figure C.3: Retrieval example for the Arctic winter season. Timespan is 1st(upper left) to 6th (lower right) December 2009

Bibliography

[1] Held, I. M., and B. J. Soden, 2000: Water vapor feedback and global warming. Annu. Rev. Energy Environ., 25, 441475

[2] K. E. Trenberth, J. Fasullo, L. Smith Trends and variability in column-integrated atmospheric water vapor. Climate Dynamics (2005) 24: 741758

[3] Hurst, D. F., S. J. Oltmans, H. Vmel, K. H. Rosenlof, S. M. Davis, E. A. Ray, E. G. Hall, and A. F. Jordan (2011), Stratospheric water vapor trends over Boulder, Colorado: Analysis of the 30 year Boulder record, J. Geophys. Res., 116, D02306, doi:10.1029/2010JD015065.

[4] Le, T. V., and W. A. Gallus Jr. (2012), Effect of an extratropical mesoscale convective system on water vapor transport in the upper troposphere/lower stratosphere: A modeling study, J. Geophys. Res., 117, D03111, doi:10.1029/2011JD016685.

[5] Susan Solomon, Karen H. Rosenlof, Robert W. Portmann, John S. Daniel, Sean M. Davis, Todd J. Sanford, and Gian-Kasper Plattner: Contributions of Stratospheric Water Vapor to Decadal Changes in the Rate of Global Warming .Science 5 March 2010: 327 (5970), 1219-1223.Published online 28 January 2010 [DOI:10.1126/science.1182488]

[6] Serreze, M. C., and C. M. Hurst. 2000. Representation of mean Arctic precipitation from NCEP-NCAR and ERA reanalysis. Journal of Climate 13(1): 182-201.

[7] Kuzmina, S. I., Johannessen, O. M., Bengtsson, L., Aniskina, O. G. and Bobylev, L. P. (2008), High northern latitude surface air temperature: comparison of existing data and creation of a new gridded data set 19002000. Tellus A, 60: 289304. doi: 10.1111/j.1600-0870.2008.00303.x

[8] Ola M Johannessen, 2008: Decreasing Arctic Sea Ice Mirrors Increasing CO_2 on Decadal Time Scale, Atmospheric and Oceanic Science Letters, 1(1), 51-56.

[9] O. M. Johannessen, K. S. Khvorostovsky, M. W. Miles, and L. P.ev, Recent ice-Sheet Growth in the Interior of Greenland. Science, vol. 310, pp. 1013-1016, 2005.

[10] C. Melsheimer and G. Heygster, Improved Retrieval of Total Water Vapor Over Polar regions From AMSU-B Microwave Radiometer Data, IEEE Trans. Geosci. Remote Sensing, vol. 46, no. 8, pp. 2307-2322, 2008.

[11] N. Selbach, Determination of total water vapour and surface emissivity of sea ice at 89 GHz, 157 GHz and 183 GHz in the arctic winter, ser. Berichte aus dem Institut fur Umweltphysik, vol. 21. Berlin, Germany: Logos-Verlag, 2003. Ph.D. dissertation.

[12] J. Miao, K. F. Knzi, G. Heygster, T. A. Lachlan-Cope, and J. Turner, Atmospheric water vapor over Antarctica derived from SSM/T2 data, J. Geophys. Res., vol. 106, no. D10, pp. 10 18710 203, 2001.

[13] J. Miao, Retrieval of atmospheric water vapor content in polar regions using space-borne microwave radiometry, Alfred-Wegener Inst. Polar Marine Res., Bremerhaven, Germany, 1998.

[14] J.Wang, P. Racette, andM. Triesky, Retrieval of precipitable water vapor by the millimeter-wave imaging radiometer in the arctic region during FIRE-ACE, IEEE Trans. Geosci. Remote Sens., vol. 39, no. 3, pp. 595 605, Mar. 2001.

[15] N. Selbach, T. J. Hewison, G. Heygster, J. Miao, A. J. McGrath, and J. Taylor, Validation of total water vapor retrieval with an airborne millimeter wave radiometer over arctic sea ice, Radio Sci., vol. 38, no. 4, p. 8061, May 2003.

[16] T. J. Hewison and S. J. English, Airborne retrievals of snow and ice surface emissivity at millimeter wavelengths, IEEE Trans. Geosci. Remote Sens., vol. 37, no. 4, pp. 18711879, Jul. 1999.

[17] Eriksson, P., S. A. Buehler, C. P. Davis, C. Emde, and O. Lemke (2011), ARTS, the atmospheric radiative transfer simulator, Version 2, J. Quant. Spectrosc. Radiat. Transfer, doi:10.1016/j.jqsrt.2011.03.001.

[18] Schweiger, A., J. Francis, J. Key, J. Intrieri, and M. Shupe, Validation of TOVS Path-P data during SHEBA, J. Geophys. Res., accepted, 2001

[19] R. Petersen, L. Cronce, W. Feltz, E. Olson and D. Helms, WVSS-II Moisture Observations:A tool for validating and monitoring satellite moisture data, http://cimss.ssec.wisc.edu/snaap/validation/

[20] Introduction to SAGE II, http://www-sage2.larc.nasa.gov/Introduction.html

[21] About GEWEX, http://www.gewex.org/gewex_overview.html

[22] L. P. Bobylev, E. V. Zabolotskikh, L. M. Mitnik,and M. L. Mitnik,Atmospheric Water Vapor and Cloud Liquid Water Retrieval over the Arctic Ocean Using Satellite Passive Microwave Sensing, IEEE TRANS GEOSCI REMOT SEN , vol. 48, no. 1, pp. 283-294, 2010, DOI: 10.1109/TGRS.2009.2028018

[23] NOAA - Earth System Research Laboratory: Global Monitoring Division http://commons.wikimedia.org/wiki/File:BAMS_climate_assess_boulder_water_vapor_2002.gif

[24] Szczodrak, M., Minnett, P. J., Gentemann, C., Long Term Comparison of AMSR-E Retrievals and Ship Based Measurements of Total Water Vapor in the Caribbean Se, American Geophysical Union, Fall Meeting 2005, abstract A33B-0907

[25] WATER VAPOR in the CLIMATE SYSTEM Special Report. December 1995, AGU website:Water vapor - a special report